

A minimum principle for microstructuring in rigid-viscoplastic crystalline solids

Sivasambu Mahesh ^a

^a*Department of Aerospace Engineering,
Indian Institute of Technology Madras, Chennai 600036. India.*

Abstract

A minimum plastic power principle is proposed for a rigid-viscoplastic crystalline domain subdivided into two sets of lath-shaped regions, called bands. The lattice orientation in each band is assumed uniform and to differ infinitesimally from that in the other band. The proposed minimum principle yields the slip activity in the bands and semi-analytical expressions for the misorientation axis and orientation of band boundaries. These band boundary characteristics are predicted for f.c.c. lattice orientations near the ideal rolling texture components. Surprisingly, it found that the predicted band boundary characteristics closely match those of microstructural features called cell block boundaries reported in the experimental literature, except when the dislocations of activated slip systems are known to interact very strongly. This suggests that except when precluded by strong dislocation interactions, continuum extremum principles may also govern microstructural characteristics.

Key words: crystal plasticity, cell block boundary, microstructure, minimum principle

1 Introduction

A characteristic substructure forms within the grains of medium to high stacking fault energy f.c.c. metals and alloy polycrystals subjected to plastic deformation. This substructure is comprised of one or two sets of approximately parallel and regularly spaced geometrically necessary dislocation boundaries (Evers et al., 2002), called cell block boundaries (CBBs). CBBs demarcate regions that are termed cell blocks, or microbands. (Steeds, 1966; Bay et al., 1989). CBBs have attracted much recent interest (Winther et al., 1997; Christoffersen and Leffers, 1998; Winther et al., 2000; Winther, 2003; Hurley and Humphreys, 2003; Hurley et al., 2003; Winther et al., 2004; Huang, 2005; Humphreys and Bate, 2006; Huang and Winther, 2007; Winther and Huang, 2007; Winther, 2008; Albou et al., 2010; Afrin et al., 2011) not only because their study can yield fundamental understanding of the substructural mechanisms that accompany plastic deformation of crystalline solids, but also because they are an important source of plastic anisotropy of grains (Peeters et al., 2002). The latter contributes to bulk plastic anisotropy, the control of which is desirable in metal forming processes (Hughes and Hansen, 1993). Understanding the microstructural arrangement of CBBs is therefore an important step toward understanding the development of plastic anisotropy in polycrystalline materials.

The sizeable literature on theories of microstructure or CBB formation permits broad classification into three approaches. The first approach phenomenologically seeks to identify patterns in experimentally observed CBB characteris-

* Corresponding author.

Email address: smahesh@iitm.ac.in (Sivasambu Mahesh).

tics. The second approach is based on the minimisation of functionals representing free energy of the crystalline domain using the methods of variational calculus. The third approach seeks to identify minimum principles that underlie CBB structure.

The crystallographic explanation for CBB orientation using the concept of duplex slip planes, due to Wert and Huang (2003), follows the first approach. They proposed that CBBs align with a pair of duplex slip planes that intersect along the axis of zero extension (the transverse direction in rolling deformation), which may not coincide with actual slip planes. Based on the set of slip systems activated during plane strain deformation of high symmetry orientations such as copper, cube, rotated cube and Goss orientations, they identified pairs of such duplex slip planes and showed that experimentally observed CBBs coincide with these duplex slip planes. The procedure of Wert and Huang (2003) to identify duplex systems is, however, limited to highly symmetric lattice orientations wherein coplanar or co-directional sets of active slip systems can be identified.

Winther and Huang (2007) have classified slip activity in f.c.c. crystals into five slip classes: single slip, coplanar slip, co-directional slip, two fold activation of easily cross-slipping systems and dependent coplanar and co-directional slip. They concluded that CBB orientation is determined only by the slip class and is independent of the macroscopically imposed deformation. Winther and Huang (2007) have given an exhaustive correspondence scheme between slip class and CBB orientation. However, their empirical correspondence scheme does not amount to a physical explanation of the observed CBB orientation.

The work of Ortiz and Repetto (1999) and Ortiz et al. (2000) pioneered the

second variational calculus based approach. They proposed a free energy functional comprised of contributions from the elastic strain energy, the plastic dissipation and the stored energy of dislocation walls that form due to plastic incompatibility between sub-domains (called laminae) and postulated its minimisation during deformation. The last contribution renders the plasticity model non-local and introduces a microstructural length scale, which is characteristic of strain-gradient plasticity. In the presence of latent hardening, homogeneous deformation of the crystalline domain by multislip does not minimise the proposed functional. Instead, the minimum is achieved by replacing homogeneous multislip activity with spatially separated single slip activities within the laminae. Dislocation walls are generated between neighbouring laminae in order to accommodate the plastic incompatibility due to different slip activities in the laminae. Significantly, these dislocation walls are assumed to be sessile, i.e., to be fixed with respect to the material. Carstensen et al. (2002) posed the finite strain evolution problem in a more general context and showed that it reduces to non-convex minimisation. Bartels et al. (2004) and Carstensen et al. (2008) applied relaxation theory to obtain the minimising lamina structure for an important class of functionals. A multi-field formulation for dissipative solids was given by Miehe (2011). Yalcinkaya et al. (2011) proposed a variant of strain-gradient plasticity for rate-dependent crystalline materials by augmenting the free energy functional with non-convex terms. Approaches for the representing dislocation wall energies have been proposed by many authors, including Gurtin (2002); Svendsen (2002) and Hurtado and Ortiz (2012). These have been evaluated by Bittencourt et al. (2003) and Nicola et al. (2005) against discrete dislocation simulations.

Non-local variational theories are able to predict the scaling of misorienta-

tion angle and the spacing of microstructural boundaries, in accord with experimental observations, when infinite latent hardening is assumed (Aubry and Ortiz, 2003; Sivakumar and Ortiz, 2004; Conti and Ortiz, 2005). However, in contrast with the literature following the first phenomenological approach (Wert and Huang, 2003; Winther et al., 1997; Winther and Huang, 2007; Albou et al., 2010), detailed comparison of predictions of misorientations across CBBs/dislocation walls and their orientations based on these theories with observations reported in the voluminous experimental literature is conspicuously absent for two reasons. First, construction of the free-energy functionals involves constitutive assumptions such as hardening induced by slip-system interactions and energy associated with dislocation walls. Their proper choice needs considerable experimental guidance, which is not yet available (Nicola et al., 2005). Second, the assumption of sessile dislocation walls in the variational theories is not realised up to plastic strains of about 0.5 in f.c.c. metals (Humphreys and Bate, 2006), so that the theories are not applicable in the small plastic strain regime (< 0.5) wherein a rich variety of CBB patterns are observed.

The third approach to predicting microstructure formation in crystalline domains is perhaps the earliest and was initiated by Chin and Wonsiewicz (1969) in an era when CBBs had not yet been experimentally observed. Chin and Wonsiewicz (1969) sought to explain the formation of coarse microstructural elements called deformation bands in wire drawn single crystals. They proposed that an inhomogeneous deformation mode of the grain will be favoured over the homogeneous deformation mode if the former were associated with less plastic power than the latter. Motivated by experimental observations of deformation band shapes, they assumed the grain to be divided into two sets

of lath-shaped ‘bands’ deforming at different rates. They also proposed that the interface between the two types of bands be so oriented as to minimise strain-rate incompatibility across the band boundaries. It is noteworthy that banding, according to Chin and Wonsiewicz (1969), was not connected to latent hardening in any way. In order to overcome the convexity of plastic power, Chin and Wonsiewicz (1969) relaxed the imposition of certain components of the strain-rate imposed on the grain. Also, Schmid’s law is not necessarily satisfied in their banded grain.

The principles of minimum plastic power and minimum deformation incompatibility across band boundaries due to Chin and Wonsiewicz (1969), were applied to explain CBB orientation and misorientation by Mahesh (2012). The most significant novelty of the latter work was that bands were assumed to be slightly misoriented with respect to each other. By this device, both shortcomings of Chin and Wonsiewicz’s banding theory were overcome: (1) the inhomogeneously deforming grain accommodated the imposed deformation exactly, and (2) Schmid’s law was strictly satisfied in both bands. Also, dislocation wall formation between inhomogeneously deforming bands did not require latent hardening.

Mahesh (2012) predicted the misorientation axes between neighbouring bands and the orientations of CBBs in the grains of an f.c.c. Taylor polycrystal subjected to uniaxial tension. The model grains were assumed rigid-plastic and rate-independent. The predictions are found to be in quantitative agreement with experimental observations of the three types of CBB structure in medium to high stacking fault energy f.c.c. materials during uniaxial tension (Huang and Hansen, 1997; Huang, 1998). Application of this method to predict CBB orientation during plane strain deformation of f.c.c. metals, however, encoun-

ters difficulties which are attributable to the assumption of rate-independence. For, during plane strain compression, grains rotate toward highly symmetric orientations, which are called the ideal rolling texture components. Rate-independent models predict non-unique solutions for the slip rates in these orientations (Van Houtte and Aernoudt, 1975). Since the predicted band characteristics depend sensitively on the slip activity selected, highly disparate sets of band characteristics are obtained from rate-independent simulations of plane strain compression.

In the present work, non-uniqueness of slip-rates in the rate-independent theory of Mahesh (2012) is overcome by considering viscoplastic rate-dependent grains (Pan and Rice, 1983; Kocks et al., 1998), for which slip activities are unique. A local theory of inhomogeneous rigid-viscoplastic grain deformation in the small plastic strain regime is developed following the third approach. CBB predictions are independent of latent hardening of slip systems, and are based on the assumption of perfectly glissile dislocations. In this respect, the present work is complementary to the variational theories of the second approach.

The present work is built upon the classical idealisation of a grain as a homogeneously deforming entity. This framework is briefly reviewed in Sec. 2 prior to the study of inhomogeneous grain deformations in Sec. 3. This analysis results in semi-analytical expressions for the misorientation axis between neighbouring bands and for the orientation of the band boundaries, given at the end of Secs. 3.5 and 3.6, respectively. In Sec. 4, predictions of these band characteristics are obtained for grains in the vicinity of five ideal texture components of the f.c.c. rolling texture and the predictions are compared with experimental observations of the misorientation axes between neighbouring microbands and

the orientation of CBBs. A discussion of the results then follows in Sec. 5.

2 The homogeneous viscoplastic grain

The classical formulation for a homogeneously deforming rigid-viscoplastic grain is outlined below following e.g., Kocks et al. (1998). Consider an ideal grain with a uniform lattice orientation specified by an orthonormal tensor $\mathbf{\Omega}$ that transforms vectors from the crystallographic coordinate system to the macroscopic coordinate system. Let \mathbf{D} denote the imposed rate of strain on this grain, which is accommodated internally by slip on S slip systems indexed by s . Let the slip plane normal and slip direction of the s -th slip system be denoted \mathbf{n}_s and \mathbf{b}_s , respectively; these satisfy $\mathbf{b}_s \cdot \mathbf{n}_s = 0$. The Schmid tensor of the s -th slip system is (Kocks et al., 1998)

$$\mathbf{m}_s = (\mathbf{b}_s \otimes \mathbf{n}_s + \mathbf{n}_s \otimes \mathbf{b}_s)/2. \quad (1)$$

Clearly, $\mathbf{m}_s = \mathbf{m}_s^T$, i.e., \mathbf{m}_s is symmetric. Also, $\text{tr } \mathbf{m}_s = \mathbf{b}_s \cdot \mathbf{n}_s = 0$, i.e., \mathbf{m}_s is traceless.

Neglecting elastic strains, the prescribed strain-rate \mathbf{D} in the grain is accommodated by slip in all the S slip systems:

$$\mathbf{D} = \sum_{s=1}^S \dot{\gamma}_s \mathbf{m}_s, \quad (2)$$

where the slip-rates $\dot{\gamma}_s$ are assumed to depend on deviatoric stress $\boldsymbol{\sigma}$ following the power-law,

$$\dot{\gamma}_s = \left| \frac{\boldsymbol{\sigma} : \mathbf{m}_s}{\tau_s} \right|^n \text{sign}(\boldsymbol{\sigma} : \mathbf{m}_s) \quad (3)$$

in a viscoplastic grain (Asaro and Needleman, 1985; Canova et al., 1988; Anand and Kothari, 1996; Miehe and Rosato, 2007). The exponent n is termed the

reciprocal rate-sensitivity and τ_s is called the critical resolved shear stress of slip system s . In Eq. (3), $\boldsymbol{\sigma} : \mathbf{m}_s = \text{tr}(\boldsymbol{\sigma} \mathbf{m}_s^T) = \text{tr}(\boldsymbol{\sigma} \mathbf{m}_s)$. Substituting Eq. (3) into Eq. (2), one obtains

$$\mathbf{D} = \sum_{s=1}^S \mathbf{m}_s \left| \frac{\boldsymbol{\sigma} : \mathbf{m}_s}{\tau_s} \right|^n \text{sign}(\boldsymbol{\sigma} : \mathbf{m}_s). \quad (4)$$

The gradient of \mathbf{D} in $\boldsymbol{\sigma}$ space is called the tangent modulus of the grain (Kocks et al., 1998):

$$\mathbf{M} := \frac{\partial \mathbf{D}}{\partial \boldsymbol{\sigma}} = \sum_{s=1}^S \frac{n \mathbf{m}_s \otimes \mathbf{m}_s}{\tau_s} \left| \frac{\boldsymbol{\sigma} : \mathbf{m}_s}{\tau_s} \right|^{n-1}. \quad (5)$$

\mathbf{M} is symmetric and positive-definite and hence, invertible. The inverse is denoted \mathbf{S} :

$$\mathbf{S} := \mathbf{M}^{-1}. \quad (6)$$

The plastic power associated with plastic deformation per unit volume is

$$P := \boldsymbol{\sigma} : \mathbf{D} = \sum_{s=1}^S \tau_s \left| \frac{\boldsymbol{\sigma} : \mathbf{m}_s}{\tau_s} \right|^{n+1} = \sum_{s=1}^S \tau_s |\dot{\gamma}_s|^{1+1/n}. \quad (7)$$

The second and third equalities in Eq. (7) are obtained using Eqs. (4) and (3), respectively. It is shown in Appendix A.1 that subject to the constraint of Eq. (2), the plastic power $P(\dot{\gamma}_1, \dot{\gamma}_2, \dots, \dot{\gamma}_S)$ is minimized by slip-rates $\dot{\gamma}_s$ given by Eq. (3).

3 The banded viscoplastic grain

3.1 Lattice orientation perturbations

Next, let the domain of the grain be divided into two alternating band-shaped regions, (1) and (2), as shown in Fig. 1. It is assumed at the outset that the two regions are of equal volume, so that their volume fractions are 1/2 each.

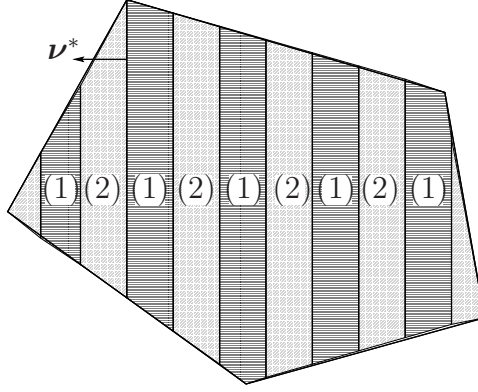


Fig. 1. Schematic diagram of a grain showing two types of bands of alternating lattice orientations, (1) and (2).

It is also assumed that the critical resolved shear stress of the s -th slip system in both bands are equal, i.e.,

$$\tau_s := \tau_s^{(1)} = \tau_s^{(2)}. \quad (8)$$

Regions (1) and (2) differ infinitesimally in their lattice orientation. The lattice orientation of region (1), $\mathbf{\Omega}^{(1)}$, assumed uniform, is obtained by rotating the lattice orientation of the homogeneous grain of Sec. 2, $\mathbf{\Omega}$, through an infinitesimal angle $d\omega$ about unit vector $\boldsymbol{\mu}$. Likewise, the lattice orientation of region (2), again assumed uniform, is obtained by giving an infinitesimal rotation $d\omega$ to $\mathbf{\Omega}$, about unit vector $-\boldsymbol{\mu}$. Thus,

$$\mathbf{\Omega}^{(1)} = \mathbf{\Omega} \exp((\boldsymbol{\mu} \times) d\omega), \quad \text{and} \quad \mathbf{\Omega}^{(2)} = \mathbf{\Omega} \exp((-\boldsymbol{\mu} \times) d\omega), \quad (9)$$

where, $(\boldsymbol{\mu} \times)$ denotes the skew-symmetric tensor that satisfies

$$(\boldsymbol{\mu} \times) \mathbf{v} = \boldsymbol{\mu} \times \mathbf{v}, \quad (10)$$

for all vectors \mathbf{v} (Gurtin, 1981). To first order in $d\omega$, Eq. (9) implies

$$\begin{aligned} \mathbf{\Omega}^{(1)} &\approx \mathbf{\Omega}(\mathbf{I} + (\boldsymbol{\mu} \times) d\omega), \quad \text{and} \\ \mathbf{\Omega}^{(2)} &\approx \mathbf{\Omega}(\mathbf{I} - (\boldsymbol{\mu} \times) d\omega). \end{aligned} \quad (11)$$

The lattice orientation perturbations imparted to the two regions produces infinitesimal variations in various lattice orientation dependent tensorial quantities (e.g., Schmid tensors, \mathbf{m}_s) associated with the two regions. In general, the infinitesimal change in the tensorial quantity \mathbf{q} when the lattice orientation is given an infinitesimal rotation $d\omega$ about the vector $\boldsymbol{\mu}$ is denoted

$$\left. \frac{d\mathbf{q}}{d\omega} \right|_{\boldsymbol{\mu}} d\omega. \quad (12)$$

If the lattice orientation is given an infinitesimal rotation $d\omega$ about the unit vector $\boldsymbol{\mu}$, the s -th Schmid tensor, \mathbf{m}_s , rotates to $(\mathbf{I} + (\boldsymbol{\mu} \times) d\omega)^T \mathbf{m}_s (\mathbf{I} + (\boldsymbol{\mu} \times) d\omega)$ following Eq. (11). The change in \mathbf{m}_s , denoted using the notation of Eq. (12) is then

$$\begin{aligned} \left. \frac{d\mathbf{m}_s}{d\omega} \right|_{\boldsymbol{\mu}} d\omega &\approx (\mathbf{I} + (\boldsymbol{\mu} \times) d\omega)^T \mathbf{m}_s (\mathbf{I} + (\boldsymbol{\mu} \times) d\omega) - \mathbf{m}_s \\ &\approx (\mathbf{m}_s (\boldsymbol{\mu} \times) - (\boldsymbol{\mu} \times) \mathbf{m}_s) d\omega. \end{aligned} \quad (13)$$

The ‘ \approx ’ symbols in Eq. (13) indicate its accuracy only to first order in $d\omega$.

In deriving Eq. (13), the property that $(\boldsymbol{\mu} \times)^T = -(\boldsymbol{\mu} \times)$ has been used. It follows that

$$\left. \frac{d\mathbf{m}_s}{d\omega} \right|_{\boldsymbol{\mu}} = \mathbf{m}_s (\boldsymbol{\mu} \times) - (\boldsymbol{\mu} \times) \mathbf{m}_s = - \left. \frac{d\mathbf{m}_s}{d\omega} \right|_{-\boldsymbol{\mu}}. \quad (14)$$

3.2 Plastic power variation to first order

It is shown below, in Eq. (30), that the plastic power of the banded grain equals that of the homogeneously deforming grain to first order.

Let $\mathbf{D}^{(1)}$ and $\mathbf{D}^{(2)}$ denote the rates of deformation in regions (1) and (2), respectively and let $\boldsymbol{\sigma}^{(1)}$ and $\boldsymbol{\sigma}^{(2)}$ denote the corresponding deviatoric stresses.

Using the notation of Eq. (12),

$$\mathbf{D}^{(1)} \approx \mathbf{D} + \left. \frac{d\mathbf{D}}{d\omega} \right|_{\boldsymbol{\mu}} d\omega, \quad \mathbf{D}^{(2)} \approx \mathbf{D} + \left. \frac{d\mathbf{D}}{d\omega} \right|_{-\boldsymbol{\mu}} d\omega, \quad (15)$$

and

$$\boldsymbol{\sigma}^{(1)} \approx \boldsymbol{\sigma} + \left. \frac{d\boldsymbol{\sigma}}{d\omega} \right|_{\boldsymbol{\mu}} d\omega, \quad \boldsymbol{\sigma}^{(2)} \approx \boldsymbol{\sigma} + \left. \frac{d\boldsymbol{\sigma}}{d\omega} \right|_{-\boldsymbol{\mu}} d\omega. \quad (16)$$

Terms of order $(d\omega)^2$ and higher have been omitted in the preceding equations.

The rate of strain imposed on the banded grain must be accommodated collectively by the two families of bands, i.e.,

$$\mathbf{D} = \frac{\mathbf{D}^{(1)} + \mathbf{D}^{(2)}}{2} = \frac{1}{2} \sum_{s=1}^S \dot{\gamma}_s^{(1)} \mathbf{m}_s^{(1)} + \frac{1}{2} \sum_{s=1}^S \dot{\gamma}_s^{(2)} \mathbf{m}_s^{(2)}, \quad (17)$$

where 1/2 is the volume fraction of the two band families, as noted in Sec. 3.1.

The second equality in Eq. (17) follows from Eq. (2). Substituting Eq. (15) into Eq. (17) gives

$$\frac{1}{2} \left. \frac{d\mathbf{D}}{d\omega} \right|_{\boldsymbol{\mu}} + \frac{1}{2} \left. \frac{d\mathbf{D}}{d\omega} \right|_{-\boldsymbol{\mu}} = \mathbf{0}. \quad (18)$$

Differentiating Eq. (4), one obtains

$$\begin{aligned} \left. \frac{d\mathbf{D}}{d\omega} \right|_{\boldsymbol{\mu}} &= \sum_{s=1}^S \left. \frac{d\mathbf{m}_s}{d\omega} \right|_{\boldsymbol{\mu}} \left| \frac{\boldsymbol{\sigma} : \mathbf{m}_s}{\tau_s} \right|^n \text{sign}(\boldsymbol{\sigma} : \mathbf{m}_s) + \\ &\quad \sum_{s=1}^S \frac{n\mathbf{m}_s}{\tau_s} \left| \frac{\boldsymbol{\sigma} : \mathbf{m}_s}{\tau_s} \right|^{n-1} \left\{ \left. \frac{d\boldsymbol{\sigma}}{d\omega} \right|_{\boldsymbol{\mu}} : \mathbf{m}_s + \boldsymbol{\sigma} : \left. \frac{d\mathbf{m}_s}{d\omega} \right|_{\boldsymbol{\mu}} \right\}. \end{aligned} \quad (19)$$

$d\mathbf{D}/d\omega|_{-\boldsymbol{\mu}}$ is obtained by simply replacing $\boldsymbol{\mu}$ by $-\boldsymbol{\mu}$ in Eq. (19):

$$\begin{aligned} \left. \frac{d\mathbf{D}}{d\omega} \right|_{-\boldsymbol{\mu}} &= \sum_{s=1}^S \left. \frac{d\mathbf{m}_s}{d\omega} \right|_{-\boldsymbol{\mu}} \left| \frac{\boldsymbol{\sigma} : \mathbf{m}_s}{\tau_s} \right|^n \text{sign}(\boldsymbol{\sigma} : \mathbf{m}_s) + \\ &\quad \sum_{s=1}^S \frac{n\mathbf{m}_s}{\tau_s} \left| \frac{\boldsymbol{\sigma} : \mathbf{m}_s}{\tau_s} \right|^{n-1} \left\{ \left. \frac{d\boldsymbol{\sigma}}{d\omega} \right|_{-\boldsymbol{\mu}} : \mathbf{m}_s + \boldsymbol{\sigma} : \left. \frac{d\mathbf{m}_s}{d\omega} \right|_{-\boldsymbol{\mu}} \right\}. \end{aligned} \quad (20)$$

Substituting Eqs. (19) and (20) in Eq. (18), using the equality of the first and third terms in Eq. (14) and recalling the tangent modulus from Eq. (5) yields

$$\mathbf{M} \left(\left. \frac{d\boldsymbol{\sigma}}{d\omega} \right|_{\boldsymbol{\mu}} + \left. \frac{d\boldsymbol{\sigma}}{d\omega} \right|_{-\boldsymbol{\mu}} \right) = \mathbf{0}. \quad (21)$$

Since \mathbf{M} is invertible, Eq. (21) implies

$$\left. \frac{d\boldsymbol{\sigma}}{d\omega} \right|_{\boldsymbol{\mu}} + \left. \frac{d\boldsymbol{\sigma}}{d\omega} \right|_{-\boldsymbol{\mu}} = \mathbf{0}. \quad (22)$$

The plastic power density P of the homogeneous grain of Sec. 2 depends only on the slip rates $\dot{\gamma}_s$, $s = 1, 2, \dots, S$, as seen from Eq. (7). The plastic power density of the banded grain generally need not equal P , on account of the infinitesimal lattice orientations $d\omega$ given to the two bands about unit vectors $\pm\boldsymbol{\mu}$. Let the infinitesimal change in plastic power be denoted $dP/d\omega|_{\pm\boldsymbol{\mu}} d\omega$. Then,

$$\begin{aligned} P + \left. \frac{dP}{d\omega} \right|_{\pm\boldsymbol{\mu}} d\omega &= \frac{\boldsymbol{\sigma}^{(1)} : \mathbf{D}^{(1)} + \boldsymbol{\sigma}^{(2)} : \mathbf{D}^{(2)}}{2} \\ &= \frac{1}{2} \sum_{s=1}^S \tau_s |\dot{\gamma}_s^{(1)}|^{1+1/n} + \frac{1}{2} \sum_{s=1}^S \tau_s |\dot{\gamma}_s^{(2)}|^{1+1/n}. \end{aligned} \quad (23)$$

It is shown in Appendix A.2 that the minimum of $P(\dot{\gamma}_1^{(1)}, \dots, \dot{\gamma}_S^{(1)}, \dot{\gamma}_1^{(2)}, \dots, \dot{\gamma}_S^{(2)})$ subject to the constraint given by Eq. (17) is attained provided

$$\dot{\gamma}_s^{(i)} = \left| \frac{\boldsymbol{\sigma}^{(i)} : \mathbf{m}_s^{(i)}}{\tau_s} \right|^n \text{sign}(\boldsymbol{\sigma}^{(i)} : \mathbf{m}_s^{(i)}), \quad i \in \{1, 2\} \quad (24)$$

and provided

$$\boldsymbol{\sigma}^{(1)} = \boldsymbol{\sigma}^{(2)}, \quad (25)$$

for $s \in \{1, 2, \dots, S\}$. Substituting Eq. (16) into Eq. (25) gives

$$\left. \frac{d\boldsymbol{\sigma}}{d\omega} \right|_{\boldsymbol{\mu}} = \left. \frac{d\boldsymbol{\sigma}}{d\omega} \right|_{-\boldsymbol{\mu}}, \quad (26)$$

which, together with Eq. (22) implies that

$$\left. \frac{d\boldsymbol{\sigma}}{d\omega} \right|_{\boldsymbol{\mu}} = \left. \frac{d\boldsymbol{\sigma}}{d\omega} \right|_{-\boldsymbol{\mu}} = \mathbf{0}. \quad (27)$$

Thus, a first order perturbation to the lattice orientation of the bands produces

no change in deviatoric stresses to first order, i.e.,

$$\boldsymbol{\sigma} = \boldsymbol{\sigma}^{(1)} = \boldsymbol{\sigma}^{(2)}. \quad (28)$$

However, substituting Eq. (27) into Eqs. (19) and (20), it is seen that the first order lattice orientation perturbation produces non-zero equal and opposite first order changes in the rates of band deformations, i.e.,

$$\left. \frac{d\mathbf{D}}{d\omega} \right|_{\boldsymbol{\mu}} = - \left. \frac{d\mathbf{D}}{d\omega} \right|_{-\boldsymbol{\mu}} = \sum_{s=1}^S \left\{ \dot{\gamma}_s \left. \frac{d\mathbf{m}_s}{d\omega} \right|_{\boldsymbol{\mu}} + \frac{n}{\tau_s} \left(\mathbf{m}_s \otimes \left. \frac{d\mathbf{m}_s}{d\omega} \right|_{\boldsymbol{\mu}} \right) \boldsymbol{\sigma} |\dot{\gamma}_s|^{1-1/n} \right\}. \quad (29)$$

Eq. (4) has been used in deriving Eq. (29).

To first order, the change in the plastic power due to the lattice orientation perturbation is

$$\begin{aligned} \left. \frac{dP}{d\omega} \right|_{\pm\boldsymbol{\mu}} d\omega &= P + \left. \frac{dP}{d\omega} \right|_{\pm\boldsymbol{\mu}} d\omega - P \\ &= \frac{\boldsymbol{\sigma}^{(1)} : \mathbf{D}^{(1)} + \boldsymbol{\sigma}^{(2)} : \mathbf{D}^{(2)}}{2} - \boldsymbol{\sigma} : \mathbf{D} \\ &= \boldsymbol{\sigma} : \frac{\mathbf{D}^{(1)} + \mathbf{D}^{(2)}}{2} - \boldsymbol{\sigma} : \mathbf{D} \\ &= 0. \end{aligned} \quad (30)$$

The third and fourth rows above follow from Eqs. (28) and (17), respectively. Thus, it has been shown that a first order perturbation of the lattice orientation produces no first order variation in the plastic power.

3.3 Plastic power variation to second order

A concise expression is derived below, in Eq. (46), for the second order perturbation of the plastic power of a grain with lattice misorientation.

It is clear from Eq. (30) that the plastic power of a banded grain may, at best,

deviate from that of the homogeneous grain to second order in $d\omega$. If so, the plastic power of the banded grain will take the form

$$P + \frac{1}{2} \frac{d^2 P}{d\omega^2} \Big|_{\pm\mu} (d\omega)^2, \quad (31)$$

where,

$$\frac{d^2 P}{d\omega^2} \Big|_{\pm\mu} := \frac{d}{d\omega} \left(\frac{dP}{d\omega} \Big|_{\pm\mu} \right) \Big|_{\pm\mu}. \quad (32)$$

Paralleling Eq. (12), the second derivative of an orientation dependent tensorial quantity, \mathbf{q} , is defined as

$$\frac{d^2 \mathbf{q}}{d\omega^2} \Big|_{\mu} = \frac{d}{d\omega} \left(\frac{d\mathbf{q}}{d\omega} \Big|_{\mu} \right) \Big|_{\mu}, \quad (33)$$

in terms of the first derivative given in Eq. (12).

Using the notation of Eq. (33),

$$\begin{aligned} \boldsymbol{\sigma}^{(1)} &= \boldsymbol{\sigma} + \frac{1}{2} \frac{d^2 \boldsymbol{\sigma}}{d\omega^2} \Big|_{\mu} (d\omega)^2, \\ \boldsymbol{\sigma}^{(2)} &= \boldsymbol{\sigma} + \frac{1}{2} \frac{d^2 \boldsymbol{\sigma}}{d\omega^2} \Big|_{-\mu} (d\omega)^2 \end{aligned} \quad (34)$$

to second order in $d\omega$. The first order terms in Eq. (34) are zero, according to Eq. (27). Substituting Eq. (34) into Eq. (28),

$$\frac{d^2 \boldsymbol{\sigma}}{d\omega^2} \Big|_{\mu} = \frac{d^2 \boldsymbol{\sigma}}{d\omega^2} \Big|_{-\mu} \quad (35)$$

is obtained. By virtue of the equality in Eq. (35), the following notation is introduced:

$$\frac{d^2 \boldsymbol{\sigma}}{d\omega^2} \Big|_{\pm\mu} := \frac{d^2 \boldsymbol{\sigma}}{d\omega^2} \Big|_{\mu} = \frac{d^2 \boldsymbol{\sigma}}{d\omega^2} \Big|_{-\mu}. \quad (36)$$

Similarly, the rate of strain in the two bands is expressible to second order in

$d\omega$ as

$$\begin{aligned} \mathbf{D}^{(1)} &= \mathbf{D} + \frac{d\mathbf{D}}{d\omega}\Big|_{\boldsymbol{\mu}} (d\omega) + \frac{1}{2} \frac{d^2\mathbf{D}}{d\omega^2}\Big|_{\boldsymbol{\mu}} (d\omega)^2, \\ \mathbf{D}^{(2)} &= \mathbf{D} + \frac{d\mathbf{D}}{d\omega}\Big|_{-\boldsymbol{\mu}} (d\omega) + \frac{1}{2} \frac{d^2\mathbf{D}}{d\omega^2}\Big|_{-\boldsymbol{\mu}} (d\omega)^2 \end{aligned} \quad (37)$$

Substituting Eq. (37) into Eq. (17) and utilising the first equality in Eq. (29) gives

$$\frac{d^2\mathbf{D}}{d\omega^2}\Big|_{\boldsymbol{\mu}} + \frac{d^2\mathbf{D}}{d\omega^2}\Big|_{-\boldsymbol{\mu}} = \mathbf{0}. \quad (38)$$

$d^2\mathbf{D}/d\omega^2|_{\boldsymbol{\mu}}$ is obtained by further differentiating Eq. (29) and applying Eqs. (35)

as

$$\begin{aligned} \frac{d^2\mathbf{D}}{d\omega^2}\Big|_{\boldsymbol{\mu}} &= \sum_{s=1}^S \left\{ \frac{d^2\mathbf{m}_s}{d\omega^2}\Big|_{\boldsymbol{\mu}} \dot{\gamma}_s + \frac{2n}{\tau_s} \left(\frac{d\mathbf{m}_s}{d\omega}\Big|_{\boldsymbol{\mu}} \otimes \frac{d\mathbf{m}_s}{d\omega}\Big|_{\boldsymbol{\mu}} \right) \boldsymbol{\sigma} + \right. \\ &\quad \frac{n(n-1)}{\tau_s^2} \mathbf{m}_s \left(\frac{d\mathbf{m}_s}{d\omega}\Big|_{\boldsymbol{\mu}} : \boldsymbol{\sigma} \right)^2 |\dot{\gamma}_s|^{1-2/n} \text{sign}(\dot{\gamma}_s) + \\ &\quad n \frac{\mathbf{m}_s \otimes \mathbf{m}_s}{\tau_s} |\dot{\gamma}_s|^{1-1/n} \frac{d^2\boldsymbol{\sigma}}{d\omega^2}\Big|_{\pm\boldsymbol{\mu}} + \\ &\quad \left. \frac{n}{\tau_s} \left(\mathbf{m}_s \otimes \frac{d^2\mathbf{m}_s}{d\omega^2}\Big|_{\boldsymbol{\mu}} \right) \boldsymbol{\sigma} |\dot{\gamma}_s|^{1-1/n} \right\}, \end{aligned} \quad (39)$$

where, following Eq. (14),

$$\begin{aligned} \frac{d^2\mathbf{m}_s}{d\omega^2}\Big|_{\boldsymbol{\mu}} &= \frac{d\mathbf{m}_s}{d\omega}\Big|_{\boldsymbol{\mu}} (\boldsymbol{\mu} \times) - (\boldsymbol{\mu} \times) \frac{d\mathbf{m}_s}{d\omega}\Big|_{\boldsymbol{\mu}} \\ &= (\mathbf{m}_s(\boldsymbol{\mu} \times) - (\boldsymbol{\mu} \times)\mathbf{m}_s) (\boldsymbol{\mu} \times) - (\boldsymbol{\mu} \times) (\mathbf{m}_s(\boldsymbol{\mu} \times) - (\boldsymbol{\mu} \times)\mathbf{m}_s). \end{aligned} \quad (40)$$

It is clear from Eq. (40) that $d^2\mathbf{m}_s/d\omega^2|_{\boldsymbol{\mu}}$ is even in $\boldsymbol{\mu}$, i.e.,

$$\frac{d^2\mathbf{m}_s}{d\omega^2}\Big|_{\pm\boldsymbol{\mu}} := \frac{d^2\mathbf{m}_s}{d\omega^2}\Big|_{\boldsymbol{\mu}} = \frac{d^2\mathbf{m}_s}{d\omega^2}\Big|_{-\boldsymbol{\mu}}. \quad (41)$$

Furthermore, a term by term consideration of the right side of Eq. (39), in light of Eq. (41), reveals that every term is even in $\boldsymbol{\mu}$. This implies that $d^2\mathbf{D}/d\omega^2|_{\boldsymbol{\mu}}$ is even in $\boldsymbol{\mu}$, i.e.,

$$\frac{d^2\mathbf{D}}{d\omega^2}\Big|_{\pm\boldsymbol{\mu}} := \frac{d^2\mathbf{D}}{d\omega^2}\Big|_{\boldsymbol{\mu}} = \frac{d^2\mathbf{D}}{d\omega^2}\Big|_{-\boldsymbol{\mu}}. \quad (42)$$

Eqs. (38) and (42) together imply that

$$\left. \frac{d^2 \mathbf{D}}{d\omega^2} \right|_{\pm\boldsymbol{\mu}} = \mathbf{0}. \quad (43)$$

Substituting Eq. (39) into Eq. (43) finally gives

$$\begin{aligned} \mathbf{M} \left. \frac{d^2 \boldsymbol{\sigma}}{d\omega^2} \right|_{\pm\boldsymbol{\mu}} = & - \sum_{s=1}^S \left\{ \left. \frac{d^2 \mathbf{m}_s}{d\omega^2} \right|_{\boldsymbol{\mu}} \dot{\gamma}_s + \frac{2n}{\tau_s} \left(\left. \frac{d\mathbf{m}_s}{d\omega} \right|_{\boldsymbol{\mu}} \otimes \left. \frac{d\mathbf{m}_s}{d\omega} \right|_{\boldsymbol{\mu}} \right) \boldsymbol{\sigma} + \right. \\ & \frac{n(n-1)}{\tau_s^2} \mathbf{m}_s \left(\left. \frac{d\mathbf{m}_s}{d\omega} \right|_{\boldsymbol{\mu}} : \boldsymbol{\sigma} \right)^2 |\dot{\gamma}_s|^{1-2/n} \text{sign}(\dot{\gamma}_s) + \\ & \left. \frac{n}{\tau_s} \left(\mathbf{m}_s \otimes \left. \frac{d^2 \mathbf{m}_s}{d\omega^2} \right|_{\boldsymbol{\mu}} \right) \boldsymbol{\sigma} |\dot{\gamma}_s|^{1-1/n} \right\}, \end{aligned} \quad (44)$$

which can be inverted to obtain the unknown tensor $d^2 \boldsymbol{\sigma} / d\omega^2|_{\pm\boldsymbol{\mu}}$.

The second order change in the plastic power due to the infinitesimal $d\omega$ lattice orientation perturbations of the two band families about $\pm\boldsymbol{\mu}$ is

$$\begin{aligned} \frac{1}{2} \left. \frac{d^2 P}{d\omega^2} \right|_{\pm\boldsymbol{\mu}} (d\omega)^2 = & \left[P + \frac{1}{2} \left. \frac{d^2 P}{d\omega^2} \right|_{\pm\boldsymbol{\mu}} (d\omega)^2 \right] - P \\ = & \frac{1}{2} \left(\boldsymbol{\sigma}^{(1)} : \mathbf{D}^{(1)} + \boldsymbol{\sigma}^{(2)} : \mathbf{D}^{(2)} \right) - \boldsymbol{\sigma} : \mathbf{D} \\ = & \frac{1}{2} \left(\boldsymbol{\sigma} + \frac{1}{2} \left. \frac{d^2 \boldsymbol{\sigma}}{d\omega^2} \right|_{\pm\boldsymbol{\mu}} (d\omega)^2 \right) : \left(\mathbf{D} + \left. \frac{d\mathbf{D}}{d\omega} \right|_{\boldsymbol{\mu}} (d\omega) + \frac{1}{2} \left. \frac{d^2 \mathbf{D}}{d\omega^2} \right|_{\pm\boldsymbol{\mu}} (d\omega)^2 \right) \\ + & \frac{1}{2} \left(\boldsymbol{\sigma} + \frac{1}{2} \left. \frac{d^2 \boldsymbol{\sigma}}{d\omega^2} \right|_{\pm\boldsymbol{\mu}} (d\omega)^2 \right) : \left(\mathbf{D} + \left. \frac{d\mathbf{D}}{d\omega} \right|_{-\boldsymbol{\mu}} (d\omega) + \frac{1}{2} \left. \frac{d^2 \mathbf{D}}{d\omega^2} \right|_{\pm\boldsymbol{\mu}} (d\omega)^2 \right) \\ - & \boldsymbol{\sigma} : \mathbf{D}. \end{aligned} \quad (45)$$

The third row in the above expression follows from substituting Eqs. (34), (35) and (37) into the second row. Expanding the last expression above and **applying Eqs.** (29) and (43), it is found that all terms of zeroth and first order in $d\omega$ vanish. The final expression for second order variation in the plastic

power accurate to second order becomes

$$\left. \frac{d^2 P}{d\omega^2} \right|_{\pm\boldsymbol{\mu}} = \mathbf{D} : \left. \frac{d^2 \boldsymbol{\sigma}}{d\omega^2} \right|_{\pm\boldsymbol{\mu}}, \quad (46)$$

where \mathbf{D} is the known imposed deformation and $d^2\boldsymbol{\sigma}/d\omega^2|_{\pm\boldsymbol{\mu}}$ is given by Eq. (44).

In summary, the plastic power perturbation depends on the misorientation vector $\boldsymbol{\mu}$, and is of second order in the lattice orientation perturbation $d\omega$.

3.4 $d^2P/d\omega^2|_{\pm\boldsymbol{\mu}}$ as a quadratic form

$d^2P/d\omega^2|_{\pm\boldsymbol{\mu}}$ given by Eq. (46) will be now be shown to be a quadratic form in $\boldsymbol{\mu}$,

$$d^2P/d\omega^2|_{\pm\boldsymbol{\mu}} = \boldsymbol{\mu} \cdot \mathbf{E} \boldsymbol{\mu}, \quad (47)$$

where \mathbf{E} is a symmetric 2-tensor. The components E_{ij} in a sample fixed orthonormal coordinate system xyz will also be obtained. Let \mathbf{e}_i , $i \in \{1, 2, 3\}$ denote the unit vectors along the x , y and z axes, respectively.

An orthonormal basis for the space of symmetric traceless matrices, due to

Leibfried et al. (1978), is recalled:

$$\begin{aligned}
[b^{(1)}] &= \frac{1}{\sqrt{2}} \begin{pmatrix} -1 & 0 & 0 \\ 0 & 1 & 0 \\ 0 & 0 & 0 \end{pmatrix}, & [b^{(2)}] &= \frac{1}{\sqrt{6}} \begin{pmatrix} -1 & 0 & 0 \\ 0 & -1 & 0 \\ 0 & 0 & 2 \end{pmatrix}, \\
[b^{(3)}] &= \frac{1}{\sqrt{2}} \begin{pmatrix} 0 & 0 & 0 \\ 0 & 0 & 1 \\ 0 & 1 & 0 \end{pmatrix}, & [b^{(4)}] &= \frac{1}{\sqrt{2}} \begin{pmatrix} 0 & 0 & 1 \\ 0 & 0 & 0 \\ 1 & 0 & 0 \end{pmatrix}, & \text{and} & \quad (48) \\
[b^{(5)}] &= \frac{1}{\sqrt{2}} \begin{pmatrix} 0 & 1 & 0 \\ 1 & 0 & 0 \\ 0 & 0 & 0 \end{pmatrix}.
\end{aligned}$$

These basis matrices are orthogonal in the sense that for $\alpha, \beta \in \{1, 2, \dots, 5\}$,

$$[b^{(\alpha)}] : [b^{(\beta)}] = \begin{cases} 1, & \text{if } \alpha = \beta, \\ 0, & \text{if } \alpha \neq \beta. \end{cases} \quad (49)$$

In the sequel, Greek indices are taken to range over $\{1, 2, \dots, 5\}$. Also, summation over repeated Greek indices is implied. In light of Eq. (49), the s -th symmetric and traceless Schmid tensor, \mathbf{m}_s , whose matrix of components in the xyz frame is denoted $[\mathbf{m}_s]_{xyz}$, may be expressed as

$$[\mathbf{m}_s]_{xyz} = m_s^{(\alpha)} [b^{(\alpha)}] \quad (50)$$

where,

$$m_s^{(\alpha)} = [\mathbf{m}_s]_{xyz} : [b^{(\alpha)}]. \quad (51)$$

It is also readily seen from Eq. (14) that $[d\mathbf{m}_s/d\omega|_{\boldsymbol{\mu}}]_{xyz}$ is symmetric and traceless. It, therefore, lies in the span of $\{[b^{(1)}], \dots, [b^{(5)}]\}$ given by Eq. (48).

Contracting both sides of Eq. (14) with $[b^{(\alpha)}]$ gives

$$\left[\frac{d\mathbf{m}_s}{d\omega} \Big|_{\boldsymbol{\mu}} \right]_{xyz} = \frac{d\mathbf{m}_s^{(\alpha)}}{d\omega} \Big|_{\boldsymbol{\mu}} [b^{(\alpha)}], \quad (52)$$

where,

$$\frac{d\mathbf{m}_s^{(\alpha)}}{d\omega} \Big|_{\boldsymbol{\mu}} = m_s^{(\beta)} \left\{ ([b^{(\beta)}](\boldsymbol{\mu} \times) - (\boldsymbol{\mu} \times)[b^{(\beta)}]) : [b^{(\alpha)}] \right\}. \quad (53)$$

In order to express Eq. (53) explicitly in terms of $\boldsymbol{\mu}$, coefficients

$$K_i^{(\alpha\beta)} = \left[[b^{(\alpha)}](\mathbf{e}_i \times) - (\mathbf{e}_i \times)[b^{(\alpha)}] \right] : [b^{(\beta)}] \quad (54)$$

are defined for $i \in \{1, 2, 3\}$. These coefficients are skew over the Greek indices, i.e., they satisfy

$$K_i^{(\alpha\beta)} = -K_i^{(\beta\alpha)}. \quad (55)$$

Taking Latin indices to range over $\{1, 2, 3\}$ and implying summation over repeated Latin indices, Eq. (53) may be expressed compactly as

$$\frac{d\mathbf{m}_s^{(\alpha)}}{d\omega} \Big|_{\boldsymbol{\mu}} = -K_i^{(\alpha\beta)} m_s^{(\beta)} \mu_i. \quad (56)$$

Analogously,

$$\begin{aligned} \frac{d^2\mathbf{m}_s^{(\alpha)}}{d\omega^2} \Big|_{\boldsymbol{\mu}} &= -K_i^{(\alpha\beta)} \frac{d\mathbf{m}_s^{(\beta)}}{d\omega} \Big|_{\boldsymbol{\mu}} \mu_i \\ &= K_i^{(\alpha\beta)} K_j^{(\beta\delta)} m_s^{(\beta)} \mu_j \mu_i, \end{aligned} \quad (57)$$

$$\left(\frac{d\mathbf{m}_s}{d\omega} \Big|_{\boldsymbol{\mu}} \otimes \frac{d\mathbf{m}_s}{d\omega} \Big|_{\boldsymbol{\mu}} \right)^{(\alpha\beta)} = K_i^{(\alpha\lambda)} K_j^{(\beta\delta)} m_s^{(\lambda)} m_s^{(\delta)} \mu_j \mu_i, \quad (58)$$

$$\left(\mathbf{m}_s \otimes \frac{d^2\mathbf{m}_s}{d\omega^2} \Big|_{\boldsymbol{\mu}} \right)^{(\alpha\beta)} = m_s^{(\alpha)} K_i^{(\beta\lambda)} K_j^{(\lambda\delta)} m_s^{(\delta)} \mu_j \mu_i, \quad (59)$$

and

$$\left(\boldsymbol{\sigma} : \frac{d\mathbf{m}_s}{d\omega} \Big|_{\boldsymbol{\mu}} \right)^2 = K_i^{(\lambda\alpha)} K_j^{(\delta\beta)} \sigma^{(\lambda)} \sigma^{(\delta)} m_s^{(\alpha)} m_s^{(\beta)}. \quad (60)$$

Substituting Eqs. (56)–(60) into Eq. (44) and substituting the result into Eq. (46) gives

$$\left. \frac{d^2 P}{d\omega^2} \right|_{\pm\boldsymbol{\mu}} = F_{ij}\mu_i\mu_j, \quad (61)$$

where,

$$\begin{aligned} F_{ij} = & -D^{(\alpha)} S^{(\alpha\lambda)} K_i^{(\lambda\nu)} K_j^{(\nu\beta)} D^{(\beta)} + 2nD^{(\alpha)} S^{(\alpha\lambda)} K_i^{(\lambda\nu)} K_j^{(\beta\delta)} \sigma^{(\delta)} \sum_{s=1}^S \frac{m_s^{(\nu)} m_s^{(\beta)}}{\tau_s} - \\ & n(n-1)D^{(\alpha)} S^{(\alpha\lambda)} K_i^{(\delta\nu)} K_j^{(\beta\delta)} \sigma^{(\nu)} \sigma^{(\delta)} \sum_{s=1}^S \frac{m_s^{(\lambda)} m_s^{(\delta)} m_s^{(\beta)}}{\tau_s^2} |\dot{\gamma}_s|^{1-2/n} \text{sign}(\dot{\gamma}_s) - \\ & D^{(\beta)} K_i^{(\nu\delta)} K_j^{(\beta\nu)} \sigma^{(\delta)}. \end{aligned} \quad (62)$$

Since $F_{ij}\mu_i\mu_j = (F_{ij} + F_{ji})\mu_i\mu_j/2$, Eq. (61) can be replaced by Eq. (47), where,

$$E_{ij} = (F_{ij} + F_{ji})/2. \quad (63)$$

3.5 Plastic power minimisation

The minimum principle of Appendix A.2 for banded grains yields the slip rates in the two band families with prescribed lattice orientations. In the present grain, the lattice orientations of the two grains are not prescribed; in particular, the axis $\boldsymbol{\mu}^*$ about which the two bands must be given lattice orientation perturbations $d\omega$ is not a priori known. In the same spirit as the minimum principle of Appendix A.2, and in light of Eq. (31), it is proposed that the optimal misorientation axis $\boldsymbol{\mu}^*$ is that which minimises $d^2 P/d\omega^2|_{\boldsymbol{\mu}}$:

$$\boldsymbol{\mu}^* = \underset{\boldsymbol{\mu}}{\text{argmin}} \left. \frac{d^2 P}{d\omega^2} \right|_{\boldsymbol{\mu}} = \underset{\boldsymbol{\mu}}{\text{argmin}} \boldsymbol{\mu} \cdot \mathbf{E}\boldsymbol{\mu}, \quad (64)$$

where the second equality follows from Eq. (47). Thus, $\boldsymbol{\mu}^*$ is the eigenvector corresponding to the smallest eigenvalue of \mathbf{E} , provided this least eigenvalue

is negative. If the least eigenvalue were non-negative, plastic power will not be reduced by banding and hence, homogeneous deformation is predicted.

3.6 Accommodation of inter-band incompatibility

A simple criterion for determining the inter-band normal, $\boldsymbol{\nu}^*$ is given presently.

Let the two families of bands (1) and (2) be rotated $d\omega$ about the axes $\pm\boldsymbol{\mu}^*$ with respect to the lattice orientation of the homogeneous grain, $\boldsymbol{\Omega}$. The infinitesimal rotations will produce infinitesimal variations $d\dot{\gamma}_s/d\omega|_{\pm\boldsymbol{\mu}^*} d\omega$ in the slip-rates in the two bands, where

$$\begin{aligned} \frac{d\dot{\gamma}_s}{d\omega}\Big|_{\boldsymbol{\mu}^*} &= \frac{d}{d\omega} \left| \frac{\boldsymbol{\sigma} : \mathbf{m}_s}{\tau_s} \right|^n \text{sign}(\boldsymbol{\sigma} : \mathbf{m}_s) \Big|_{\boldsymbol{\mu}^*} = \frac{n}{\tau_s} |\dot{\gamma}_s|^{1-1/n} \left(\boldsymbol{\sigma} : \frac{d\mathbf{m}_s}{d\omega} \Big|_{\boldsymbol{\mu}^*} \right), \quad \text{and} \\ \frac{d\dot{\gamma}_s}{d\omega}\Big|_{-\boldsymbol{\mu}^*} &= \frac{d}{d\omega} \left| \frac{\boldsymbol{\sigma} : \mathbf{m}_s}{\tau_s} \right|^n \text{sign}(\boldsymbol{\sigma} : \mathbf{m}_s) \Big|_{-\boldsymbol{\mu}^*} = \frac{n}{\tau_s} |\dot{\gamma}_s|^{1-1/n} \left(\boldsymbol{\sigma} : \frac{d\mathbf{m}_s}{d\omega} \Big|_{-\boldsymbol{\mu}^*} \right). \end{aligned} \quad (65)$$

Eq. (3) has been used in obtaining the first equality in both rows of the above equation. Eqs. (65) and (14), together imply that

$$\frac{d\dot{\gamma}_s}{d\omega}\Big|_{\boldsymbol{\mu}^*} - \frac{d\dot{\gamma}_s}{d\omega}\Big|_{-\boldsymbol{\mu}^*} = \frac{2n}{\tau_s} |\dot{\gamma}_s|^{1-1/n} \left(\boldsymbol{\sigma} : \frac{d\mathbf{m}_s}{d\omega} \Big|_{\boldsymbol{\mu}^*} \right). \quad (66)$$

Inhomogeneity of slip-rates will engender inter-band displacement incompatibility, which in turn, must be accommodated by geometrically necessary dislocations (Ashby, 1970; Cermelli and Gurtin, 2001) in order to preserve continuity of the total deformation.

Regarding the homogeneous grain of uniform lattice orientation $\boldsymbol{\Omega}$ as the reference geometrically necessary dislocation free state ($\mathbf{G} = \mathbf{0}$), the rate of accumulation of geometrically necessary dislocations, $\dot{\mathbf{G}}$, is given by Cermelli

and Gurtin (2001, Eq. (11.11)) as

$$\dot{\mathbf{G}} = - \sum_{s=1}^S (\mathbf{n}_s \times \nabla_L \dot{\gamma}_s) \otimes \mathbf{b}_s, \quad (67)$$

where ∇_L denotes the gradient transported to the lattice. Since slip is homogeneous within each band, $\nabla_L \dot{\gamma}_s = \mathbf{0}$ within each band. Any geometrically necessary dislocation density can only arise at the inter-band boundaries. Let the inter-band boundaries, denoted S , be planar with normal $\boldsymbol{\nu}$ and be of negligible thickness. Then,

$$\nabla_L \dot{\gamma}_s = \boldsymbol{\nu} \left(\left. \frac{d\dot{\gamma}_s}{d\omega} \right|_{\boldsymbol{\mu}^*} - \left. \frac{d\dot{\gamma}_s}{d\omega} \right|_{-\boldsymbol{\mu}^*} \right) \delta(S - \mathbf{x}), \quad (68)$$

where $\delta(S - \mathbf{x})$ denotes the Dirac delta function that vanishes everywhere except at the inter-band boundaries, and $\boldsymbol{\nu}$ is directed from band (1) to band (2).

The geometrically necessary dislocation density per unit surface area is obtained by substituting Eq. (68) into Eq. (67) as

$$\begin{aligned} \left. \frac{d\dot{\mathbf{G}}}{d\omega} \right|_{\boldsymbol{\mu}} &= \boldsymbol{\nu} \times \sum_{s=1}^S \left(\left. \frac{d\dot{\gamma}_s}{d\omega} \right|_{\boldsymbol{\mu}^*} - \left. \frac{d\dot{\gamma}_s}{d\omega} \right|_{-\boldsymbol{\mu}^*} \right) \mathbf{n}_s \otimes \mathbf{b}_s, \\ &= \boldsymbol{\nu} \times \sum_{s=1}^S \left(\frac{2n}{\tau_s} |\dot{\gamma}_s|^{1-1/n} \left(\boldsymbol{\sigma} : \left. \frac{d\mathbf{m}_s}{d\omega} \right|_{\boldsymbol{\mu}^*} \right) \right) \mathbf{n}_s \otimes \mathbf{b}_s \\ &= \boldsymbol{\nu} \times \mathbf{A}. \end{aligned} \quad (69)$$

The second row above is obtained by substituting Eq. (66) into the first row. Also, the cross product between vector $\boldsymbol{\nu}$ and 2-tensor \mathbf{A} is given in component form as $(\boldsymbol{\nu} \times \mathbf{A})_{ij} = e_{ipq} \nu_p A_{qj}$, where e_{ipq} denotes components of the alternating tensor.

If the dislocation density at a point is given by the scalar ρ , a reasonable approximation for the stored energy density is given by $\rho G b^2 / 2$, where G

denotes the elastic shear modulus and b the Burgers vector (Hirth and Lothe, 1992). The square-norm

$$d\dot{G}/d\omega\Big|_{\boldsymbol{\mu}} : d\dot{G}/d\omega\Big|_{\boldsymbol{\mu}} = \mathbf{A} : \mathbf{A} - \boldsymbol{\nu} \cdot \mathbf{A}\mathbf{A}^T\boldsymbol{\nu}. \quad (70)$$

is proportional to the square of the rate of dislocation storage per unit inter-band surface area (Nye, 1953). Since G and b are uniform throughout the grain, the energy storage per unit inter-band surface area is approximately $\rho G b^2 (\mathbf{A} : \mathbf{A} - \boldsymbol{\nu} \cdot \mathbf{A}\mathbf{A}^T\boldsymbol{\nu})/2$.

In the spirit of the minimum principle of Appendix A.2 it is proposed that the optimal band normal $\boldsymbol{\nu}^*$ is oriented so as to minimise the stored energy. It is clear from the right side of Eq. (70) that the stored energy is minimised if $\boldsymbol{\nu}^*$ is parallel to the eigenvector of $\mathbf{A}\mathbf{A}^T$ that corresponds to the largest eigenvalue.

4 Results

4.1 Polycrystal simulations

The present theory is now applied to predict the misorientation axis, $\boldsymbol{\mu}^*$, across band boundaries and their normals, $\boldsymbol{\nu}^*$ in the grains of model f.c.c. polycrystals deforming by $\{111\}\langle 110\rangle$ slip. For this purpose, the present theory is implemented within a binary-tree based model of a polycrystal (Mahesh, 2009). In this model, sub-aggregates are represented as the nodes of a binary tree. The lowest (leaf) nodes of the binary tree represent grains. Higher binary tree nodes represent increasingly larger sub-aggregates of grains, culminating with the root of the tree, which represents the entire polycrystalline aggregate. Thus, unlike in the Taylor (1938) or the self-consistent (Lebensohn and

Tomé, 1993) models, interactions between neighbouring grains are directly but approximately accounted for in the binary-tree based model.

Component	(ND)[RD]	Euler angles		
		ϕ_1	Φ	ϕ_2
Brass	(110)[1 $\bar{1}$ 2]	54.74°	90.00°	45.00°
Copper	(112)[11 $\bar{1}$]	-90.00°	35.26°	45.00°
Cube	(001)[100]	0.00°	0.00°	0.00°
Goss	(110)[001]	90.00°	90.00°	45.00°
S	(123)[63 $\bar{4}$]	-58.98°	36.70°	26.57°

Table 1

The ideal f.c.c rolling texture components presently studied.

For the purpose of determining $\boldsymbol{\mu}^*$ and $\boldsymbol{\nu}^*$, attention is restricted to the part of the orientation space close to the ideal f.c.c. rolling texture components listed in Tab. 1. For each of the ideal orientations, a uniform random sample of 256 grains disoriented at most 15° from the ideal orientation or from one of its orthonormal sample symmetric variants is generated. A balanced binary tree model of the polycrystal is then built out of these grains (Mahesh, 2009). This approach to studying the vicinity of the ideal texture components in lattice orientation space follows that adopted by Kuroda and Tvergaard (2007) in their study of shear banding. The 15° disorientation condition presently adopted mimicks that used in the experimental works of Hurley et al. (2003) and Huang and Winther (2007) for defining lattice orientations near the ideal texture components. The $\{111\}$ pole figures of the five polycrystals whose grains are oriented near the five ideal orientations are shown in the left column of

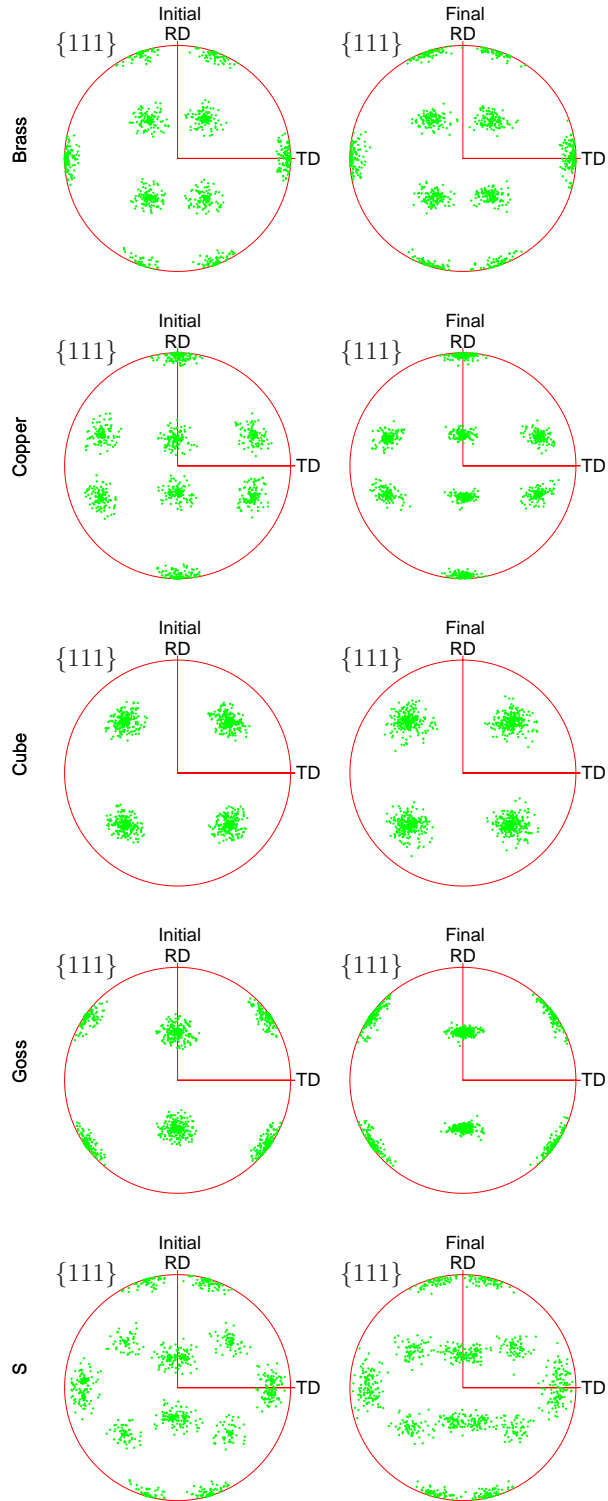


Fig. 2. $\{111\}$ pole figures showing the initial ($\epsilon_{vM} = 0$) and final ($\epsilon_{vM} = 0.25$) texture of the five polycrystals, each comprised of 256 grains, presently studied.

Fig. 2. All pole figures presented in this work use equal area projection (Kocks et al., 1998).

Rolling deformation to a von Mises strain of 0.25, which amounts to a rolling reduction of 22%, is simulated. The three principal orthogonal directions in the rolling process are the rolling direction (RD), transverse direction (TD), and normal direction (ND). A sample coordinate system, xyz , which coincides with RD–TD–ND is introduced. The macroscopic strain-rate

$$[\bar{\mathbf{D}}]_{xyz} = \begin{pmatrix} 1 & 0 & 0 \\ 0 & 0 & 0 \\ 0 & 0 & -1 \end{pmatrix} \quad (71)$$

is applied to the root node of the binary-tree based model, which represents the entire polycrystal. It is to be noted that the strain-rate of an individual grain in the binary-tree based model, \mathbf{D} , may differ significantly from the macroscopically imposed deformation rate $\bar{\mathbf{D}}$ on the polycrystal due to intragranular interactions. The post deformation $\{111\}$ textures are shown in the second column of Fig. 2. It is seen that in all five cases, the final texture is similar to the initial texture, which indicates texture stability.

No hardening of slip systems is assumed. Thus in all grains,

$$\tau_s = 1, \quad \forall s \in \{1, 2, \dots, S = 12\} \quad (72)$$

throughout the simulations.

4.2 Ideal orientations

The present predictions are now juxtaposed with reports on the observed characteristics of CBBs from the experimental literature in order to highlight similarities and differences between them.

4.2.1 Macroscopic vs. crystallographic preference

In a rolled copper polycrystal, Christoffersen and Leffers (1998) observed that regardless of the grain lattice orientation, CBBs preferentially align parallel to the maximum shear stress (MSS) planes. They suggested that CBB orientation is determined mostly by the macroscopically imposed deformation and is independent of the grain's lattice orientation. This viewpoint, which holds the *macroscopic influence* to dominate, has been supported by Hurley and Humphreys (2003); Hurley et al. (2003) and Humphreys and Bate (2006). In particular, these authors have advanced the view that CBBs have no particular bias for alignment with $\{111\}$ planes. A contrary view, based on transmission electron microscopy, advanced by Winther et al. (1997, 2000); Winther (2003); Winther et al. (2004); Huang (2005); Huang and Winther (2007); Winther and Huang (2007) and Winther (2008), suggests that CBB orientation is determined by the *crystallographic influence*: the more slip concentrated in a single $\{111\}$ slip plane, the closer the CBB aligns with it. In this view, the proximity of the observed CBBs to MSS planes simply reflects the orientation of the activated slip systems.

The pole figures of Fig. 3 depict misorientation axes across band boundaries, $\boldsymbol{\mu}^*$, (columns (a) and (b)) and band boundary normals, $\boldsymbol{\nu}^*$, (columns (c) and

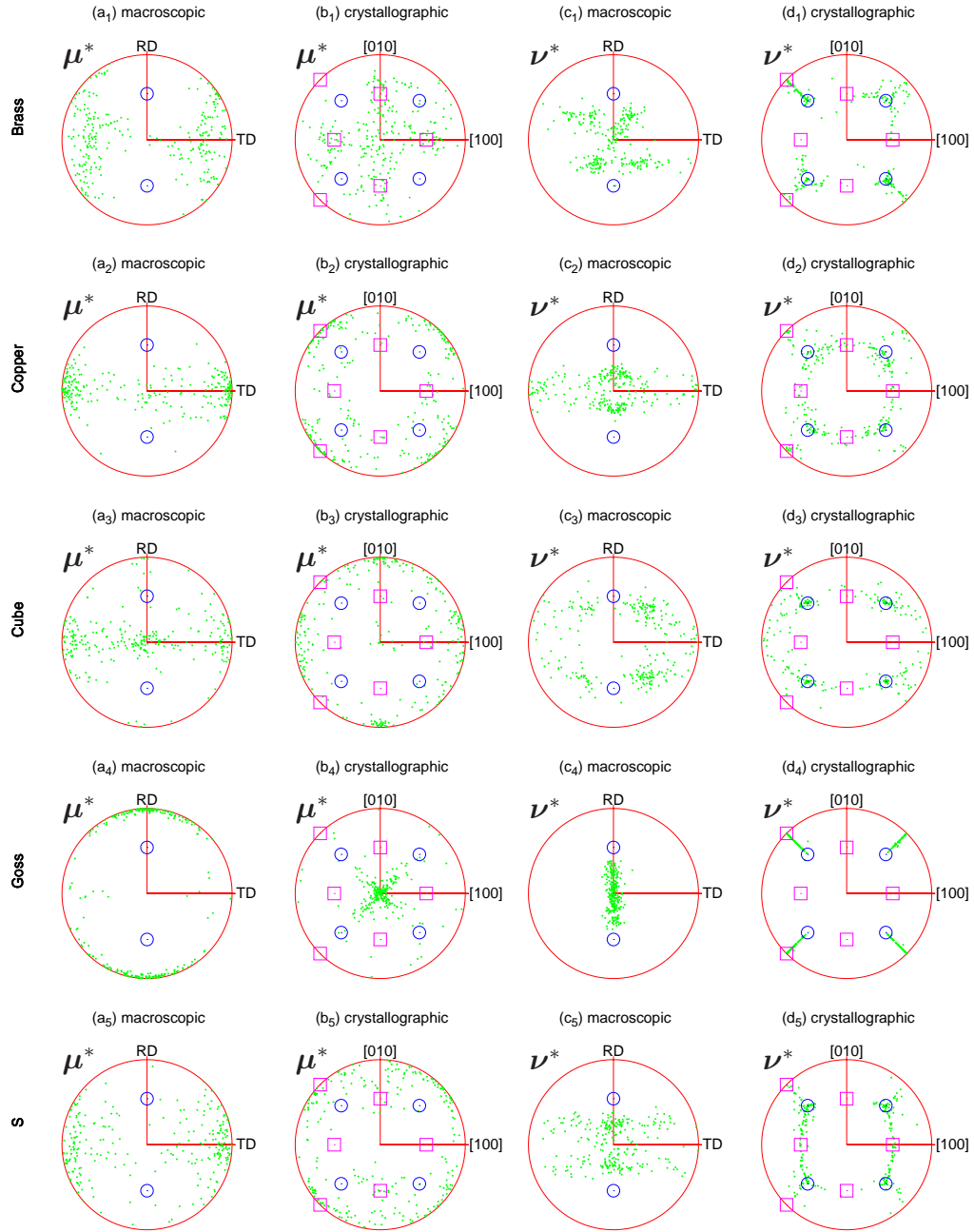


Fig. 3. Misorientation axes μ^* predicted across band boundaries in the macroscopic (column (a)) and crystallographic (column (b)) coordinate systems. Band boundary normals ν^* in the macroscopic (column (c)) and crystallographic (column (d)) coordinate systems near the brass, copper, cube, Goss, and S orientations.

(d)) in the macroscopic (columns (a) and (c)) and crystallographic (columns (b) and (d)) coordinate systems. Each row in Fig. 3 corresponds to one of the five ideal orientations listed in Tab. 1. There are 256 dots in each pole figure, one for $\boldsymbol{\mu}^*$ or $\boldsymbol{\nu}^*$ in one grain. Circles in columns (a) and (c) identify the normal to the MSS planes, i.e., the angle bisector of \pm RD and ND. Circles and squares in columns (b) and (d) identify the $\{110\}$ and $\{111\}$ crystallographic plane normals, respectively.

No macroscopic or crystallographic preference for $\boldsymbol{\mu}^*$ or $\boldsymbol{\nu}^*$ is built into the present model. Nevertheless, it is seen from column (a) in Fig. 3 that the predicted $\boldsymbol{\mu}^*$ in the brass, copper and S orientations are concentrated close to TD, while that of the cube orientation is concentrated near TD and ND and that of Goss is concentrated near RD. RD, TD and ND represent the principal directions of the macroscopically imposed deformation. Except in the case of the Goss orientation, the $\boldsymbol{\mu}^*$ concentration along particular crystallographic directions, as seen in column (b) of Fig. 3 is weaker. It thus appears that the misorientation axes across the predicted CBBs have a macroscopic character. On the other hand, column (d) of Fig. 3 shows that the predicted CBBs $\boldsymbol{\nu}^*$ fall predominantly on $\{111\}$ or $\{110\}$ planes. No strong preference for the macroscopic RD, TD and ND directions is seen in column (c). It may thus be concluded that the crystallographic influence on the predicted $\boldsymbol{\nu}^*$ is stronger than the macroscopic influence.

The predicted band boundary misorientation $\boldsymbol{\mu}^*$ and orientation $\boldsymbol{\nu}^*$ given in Fig. 3 are now compared with experimental observations of cell block boundaries (CBB) reported in the literature for each of the five ideal orientations below.

4.2.2 Brass orientation

It is seen from Fig. 3 (a₁) that predicted misorientation axes are distributed close to TD. This accords well with an experimental observation of Albou et al. (2010) who noted in a channel die compressed Brass oriented single crystal Al alloy that “the vast majority of the disorientation axes are situated in the vicinity of the TD axis, but, more specifically, about 10–20° off TD towards RD” after effective strains of 0.15 and 0.5. The symmetric spread of predicted μ^* about the TD in Fig. 3 (a₁) is because the present brass polycrystal contains grains oriented close to all four sample symmetry variants (Kocks et al., 1998) of the ideal brass orientation.

Fig. 3 (d₁) shows that most band boundary ν^* are predicted to be aligned close to $\{111\}$ slip planes. This prediction compares well with the observations of Huang and Winther (2007). In nine grains of an Al polycrystal oriented within 15° of the brass orientation, they found the CBB plane and the slip plane traces in the RD-ND section to be within 7°.

In Fig. 3 (c₁) and (d₁), ν^* in some grains is also predicted to align with certain $\{110\}$ planes, which coincide with ND. CBBs with these orientations have not been reported at small rolling reductions, even though they are common at high rolling reductions (Wróbel et al., 1994; Albou et al., 2010).

4.2.3 Copper orientation

Fig. 3 (a₂) shows that in the copper orientation, the predicted band boundary misorientation axis μ^* is closely aligned with TD, in agreement with experimental observations of Wagner et al. (1995) in rolled copper oriented Cu,

Cu-Al alloy and Al single crystals. The latter experimental observation is also confirmed by the observations of Godfrey et al. (1998) in pure Al subjected to channel-die compression.

In pure Cu, Morii et al. (1985) and Wagner et al. (1995) have reported the observation of CBBs parallel to the slip plane of the active $\{111\}$ coplanar systems in copper-oriented single crystals. Godfrey et al. (1998) have also observed a set of coarse CBBs parallel to the slip plane of the coplanar systems in parts of a copper-oriented Al single crystals channel-die compressed to $\epsilon_{vM} = 0.5$. The presently predicted CBBs parallel to $\{111\}$, shown in Fig. 3 (c₂) and (d₂) coincide with this experimentally observed CBB orientation. Band boundaries of $\{001\}$ orientation are not predicted presently.

4.2.4 *Cube orientation*

In an Al single crystal cold rolled 15%, Liu and Hansen (1998) observed a microstructure comprised of dislocation cells with some CBBs. They found lattice rotations predominantly about TD across the CBBs. The predicted misorientation axes, $\boldsymbol{\mu}^*$, concentrate near TD and to a lesser degree, near ND, as seen from Fig. 3 (a₃). The prediction that $\boldsymbol{\mu}^* \parallel \text{TD}$, accords well with the observations of Liu and Hansen (1998). However, the latter prediction of alignment with ND has, to our knowledge, not been experimentally observed. Also, the band boundaries are predicted to be closely aligned with $\{111\}$ planes, as seen in Fig. 3 (d₃), which agrees with the observations of Liu and Hansen in their 15% reduced specimen. In nearly cube oriented grains in polycrystalline Al, Huang and Winther (2007) report occasional CBBs oriented along (101) and ($\bar{1}01$). This CBB alignment is not presently predicted.

At larger plane strain reductions, cube oriented single crystals are known to sub-divide into matrix bands (Akef and Driver, 1991; Liu and Hansen, 1998). The matrix bands rotate away from the cube orientation. Since matrix banding is not accounted for in the present calculations, the present predictions cannot be compared with experimental observations on cube oriented single crystals at large reductions.

4.2.5 Goss orientation

In the vicinity of the Goss orientation, the misorientation axis across the band boundaries is predicted to be aligned close to RD for most grains, and close to TD for a few grains, in Fig. 3 (a₄). The former alignment is predicted for grains disoriented 2°–15° from the ideal Goss orientation while the latter set of grains are those whose initial lattice orientations are within about 2° of the ideal Goss orientation. In experimental observations of Ni single crystals subjected to plane strain compression to effective strain 0.35 (Afrin et al., 2012), the orientation spread is found to have a minor component along RD ($\pm 3.5^\circ$) and a major component along TD ($\pm 7.5^\circ$). A similar conclusion was also obtained in rolled Al single crystals by Liu et al. (2000). If it assumed that the initial lattice orientation of the experimental single crystals closely matches the ideal Goss orientation, it can be concluded that the presently predicted alignment of $\boldsymbol{\mu}^* \parallel \text{TD}$ agrees with experimental reports.

Some of the band boundaries are predicted to be normal to the $\{111\}$ planes in Fig. 3 (d₄), while others are distributed between $\{111\}$ and $\{110\}$ planes. Again, in near ideal Goss oriented grains, $\boldsymbol{\nu}^* \parallel \{111\}$ is predicted, while in the grains oriented further from ideal Goss, $\boldsymbol{\nu}^* \parallel \text{ND}$ is predicted, as shown

in Fig. 3 (c₄). The predicted alignment of band boundaries with {111} planes is in accord with experimental observations of Afrin et al. (2011, 2012) in Ni single crystals, Liu et al. (2000) in Al single crystals, Ananthan et al. (1991) in the near Goss grains of a copper polycrystal and Hurley et al. (2003) in the grains of an Al-Mg polycrystal.

4.2.6 *S orientation*

The predicted misorientation axis, $\boldsymbol{\mu}^*$, is oriented close to TD and a predicted boundary normals, $\boldsymbol{\nu}^*$ are aligned close to {111} planes, as shown in Figs. 3 (a₆) and (d₆), respectively. Although experimental measurements of the misorientation axis across CBBs to compare $\boldsymbol{\mu}^*$ with are lacking, the predicted $\boldsymbol{\nu}^*$ agrees with the orientation of CBBs in an aluminum alloy (Winther et al., 2004; Huang and Winther, 2007).

In addition to the crystallographically aligned CBBs, Winther et al. (2004); Huang and Winther (2007) and Lin et al. (2009) have also reported the observation of a set of CBBs aligned with crystallographic {131} planes. Boundaries of this alignment not predicted for reasons discussed below.

4.2.7 *Unpredicted cell-block boundaries*

It emerges from the results presented in Secs. 4.2.2–4.2.6 that while most experimentally observed CBBs are predicted, the following three are not:

- (i) {001} CBBs in copper oriented Al single crystals and grains (Godfrey et al., 1998; Huang and Winther, 2007; Lin et al., 2009),
- (ii) {110} CBBs in cube oriented Al grains (Huang and Winther, 2007), and

(iii) $\{131\}$ CBBs in S oriented Al alloy grains (Huang and Winther, 2007; Lin et al., 2009).

It is important to note that boundaries of type (i) are not observed in copper oriented Cu single crystals or grains (Morii et al., 1985; Wagner et al., 1995). A commonality amongst the three unpredicted boundaries above is that each of them occurs in an ideal orientation wherein cross-slip systems are activated¹. Moreover, each of the unpredicted boundary planes listed above contains the cross-slip direction.

Dislocations on cross-slip systems in f.c.c. materials form the strongest dislocation junctions through collinear interactions, as shown by Madec et al. (2003) using dislocation dynamics simulations. Furthermore, cross-slip is easier in higher stacking fault energy materials such as Al than in lower stacking fault energy materials such as Cu (Hirth and Lothe, 1992). These facts suggest that the three unpredicted CBBs listed above are nucleated by sessile dislocation segments formed out of collinear dislocation reactions in high stacking fault energy Al or Al alloys. The present work, being based on the assumption of non-reacting dislocations does not predict these CBB orientations as it is unable to capture the effect of CBB nucleation from sessile dislocation locks or junctions.

¹ Distinct slip systems s_1 and s_2 are called cross-slip systems if they share the same slip direction, i.e., $\mathbf{b}_{s_1} = \mathbf{b}_{s_2}$. The common slip direction is called the cross-slip direction.

5 Discussion

In the physical grain, CBBs form by the collective motion of dislocations, which has not, however, been explicitly treated presently. Instead, the present minimum power principle determines CBB characteristics: $\boldsymbol{\mu}^*$ (Sec. 3.5), and $\boldsymbol{\nu}^*$ (Sec. 3.6). Thus, the present treatment has tacitly assumed that the requisite dislocations can be nucleated and the collective dislocation motions required to achieve the two aforementioned minima will be physically realised. This assumption is clearly satisfied in highly symmetric f.c.c. polycrystals which have a large number of slip systems as seen in Secs. 4.2.2–4.2.6, except when dislocation interactions become very strong, as noted in Sec. 4.2.7. It, however, seems unlikely that this assumption will be met in lower symmetry materials, such as h.c.p. polycrystals.

Infinitesimal misorientations $d\omega$ are essential for CBB formation according to the present theory (Sec. 3). Small misorientations in physical grains occur across incidental dislocation boundaries both in annealed and plastically deformed grains (Bay et al., 1989; Kuhlmann-Wilsdorf and Hansen, 1991). The misorientation angle across these boundaries is typically of the order of a few degrees, and the misorientation axis across these boundaries is uniformly distributed over the surface of the unit sphere (Hughes et al., 1997, 1998; Godfrey and Hughes, 2000). Incidental dislocation boundaries can thus be regarded as the physical source of lattice orientation perturbations $d\omega$ about the unit vector $\boldsymbol{\mu}$, in Secs. 3.5 and 3.6. Then, the key hypothesis of Sec. 3.5 may be restated as follows: Segments of incidental dislocation boundaries, whose misorientation axes happen to coincide with $\boldsymbol{\mu}^*$ are most favoured as nuclei of geometrically necessary CBBs.

The theory is based on the assumption that CBB orientations at any stage of the deformation depends only the instantaneous slip activity in the grain (Sec. 3); it is assumed that the deformation history does not influence CBB orientations. This amounts to assuming that dislocations are glissile, so that CBBs can move freely with respect to the material and achieve the configurations that satisfy the present minimum power principle. The assumption of glissile dislocations is reasonable in the early stages of plastic deformation when the dislocation density, and hence, the probability of forming sessile dislocation junctions, is relatively small. In this regime, CBBs are experimentally known to orient in accord with the instantaneous slip activity (Christoffersen and Leffers, 1998; Humphreys and Bate, 2006; Albou et al., 2010). However, with increasing deformation (e.g., for $\epsilon_{vM} > 0.5$ in high stacking fault energy f.c.c. materials), the dislocation density increases, and an increasing number of dislocation segments become sessile through dislocation reactions (McCabe et al., 2004). Dislocation walls comprised largely of such sessile dislocation segments orient themselves in accord with the evolving grain shape; e.g., they align parallel to the rolling plane, when the grain is subjected to high rolling deformation (Albou et al., 2010). Thus, with increasing strain, the present minimum power principle will become increasingly invalid as the criterion that determines CBB characteristics, and the assumptions underlying the variational theories described in Sec. 1 will be realised.

Another consequence of the assumption of glissile dislocations is that the present theory is local and is unable to predict the accumulation of dislocation density or disorientation with strain across CBBs. Since CBBs are presently assumed to be instantaneously nucleated from incidental dislocation boundaries throughout the deformation, the initial geometrically necessary disloca-

tion density $\mathbf{G} = \mathbf{0}$ (Eq. (69)). Predictions of the accumulation of dislocation density or disorientation with strain are meaningful only for CBBs comprised of sessile dislocation segments fixed with respect to the material, e.g., Ortiz et al. (2000); Carstensen et al. (2002, 2008).

In obtaining the optimal μ^* , the rate of increase of stored energy associated with accommodation of the incompatibility across the band boundaries has been neglected. Thus, it has been tacitly assumed that the former component of energy is much smaller than the reduction in plastic power of the grain by banding. This assumption can be expected to be valid only for dislocation boundaries such as CBBs across which the misorientation angle is small. Across dislocation boundaries with large misorientation angles, e.g., deformation bands and shear bands, compatibility of deformation must be explicitly imposed, as in Mahesh (2006) and Arul Kumar and Mahesh (2012).

As noted in Sec. 1, the plastic anisotropy of grains can be inferred from the preferred orientations of CBBs. The present methodology for predicting CBB orientations offers a computationally efficient methodology to incorporate plastic anisotropy due to dislocation structures at the sub-granular length scale into polycrystal plasticity simulations (Kocks et al., 1998). The computational efficiency arises because CBB orientation prediction using present theory only involves the computation of the eigenspace of two symmetric 3×3 matrices, which are analytically obtained. This may be contrasted with the several orders of magnitude greater computational resources required to obtain CBB orientation predictions from methods such as dislocation dynamics (Bulatov and Cai, 2006).

6 Conclusion

Grains are modelled as crystalline domains divided into lath shaped regions, each of which is infinitesimally misoriented relative to its neighbours. The misorientation axis of band boundaries is derived using a minimum plastic power principle, and the orientation of these boundaries is derived by minimising the geometrically necessary dislocation density within grains. The predicted misorientation axes and orientations of band boundaries are compared with experimental observations pertaining to a type of dislocation boundary, called the cell block boundary, reported in the literature. Good agreement is found for the majority of cases, which is surprising in that no account is taken of the mechanisms of the motion of single dislocations and groups of dislocations. The cases wherein agreement between theoretical predictions and experimental observations break down pertain to the cases wherein the dislocations generated in the course of slip are known to react particularly strongly. This suggests that the hypothesised energy based criteria indeed govern CBB properties to first order. However, correction for strong dislocation interactions is needed if the predictions are to be applicable universally.

Acknowledgment: The author thanks Dr. Ishan Sharma, IIT Kanpur for valuable discussions and gratefully acknowledges use of the POLE software developed by Dr. C. N. Tomé for generating all the pole figures presented here. Funding was provided by the Indira Gandhi Centre for Atomic Research, Kalpakkam and by the Board of Research in Nuclear Sciences.

References

- Afrin, N., Quadir, M., Xu, W., Ferry, M., 2012. Spatial orientations and structural irregularities associated with the formation of microbands in a cold deformed goss oriented ni single crystal. *Acta Materialia* 60 (18), 6288 – 6300.
- Afrin, N., Quadir, M. Z., Bassman, L., Driver, J. H., Albou, A., Ferry, M., 2011. The three-dimensional nature of microbands in a channel die compressed Goss-oriented Ni single crystal. *Scripta Mater.* 64 (3), 221–224.
- Akef, A., Driver, J. H., 1991. Orientation splitting of cube-oriented face-centered cubic crystals in plane strain compression. *Mat. Sci. Eng. A* 132, 245–255.
- Albou, A., Driver, J. H., Maurice, C., 2010. Microband evolution during large plastic strains of stable $\{110\}\langle 112 \rangle$ Al and Al-Mn crystals. *Acta mater* 58, 3022–3034.
- Anand, L., Kothari, M., 1996. A computational procedure for rate-independent crystal plasticity. *J. Mech. Phys. Solids* 44 (4), 525–558.
- Ananthan, V. S., Leffers, T., Hansen, N., 1991. Characteristics of 2nd generation microbands in cold-rolled copper. *Scripta metall. mater.* 25, 137–142.
- Arul Kumar, M., Mahesh, S., 2012. Banding in single crystals during plastic deformation. *International Journal of Plasticity* 36, 15 – 33.
- Asaro, R. J., Needleman, A., 1985. Overview 42. Texture development and strain-hardening in rate dependent polycrystals. *Acta metall.* 33 (6), 923–953.
- Ashby, M. F., 1970. The deformation of plastically non-homogeneous materials. *Phil. Mag.* 21 (170), 399.
- Aubry, S., Ortiz, M., 2003. The mechanics of deformation-induced subgrain

- dislocation structures in metallic crystals at large strains. *Proc. R. Soc. Lond A* 459, 3131–3158.
- Bartels, S., Carstensen, C., Hackl, K., Hoppe, U., 2004. Effective relaxation for microstructure simulations: algorithms and applications. *Comput. Meth. Appl. Mech. Eng.* 193 (4851), 5143 – 5175.
- Bay, B., Hansen, N., Kuhlmann-Wilsdorf, D., 1989. Deformation structures in lightly rolled pure aluminum. *Mater. Sci. Eng. A* 113, 385–397.
- Bittencourt, E., Needleman, A., Gurtin, M., Van der Giessen, E., 2003. A comparison of nonlocal continuum and discrete dislocation plasticity predictions. *J. Mech. Phys. Solids* 51 (2), 281–310.
- Bulatov, V., Cai, W., 2006. Computer simulations of dislocations. Vol. 3. Oxford University Press.
- Canova, G. R., Fressengeas, C., Molinari, A., Kocks, U. F., 1988. Effect of rate sensitivity on slip system activity and lattice rotation. *Acta Metall.* 38 (8), 1961–1970.
- Carstensen, C., Conti, S., Orlando, A., 2008. Mixed analytical-numerical relaxation in finite single-slip crystal plasticity. *Continuum Mech. Thermodynamics* 20 (5), 275–301.
- Carstensen, C., Hackl, K., Mielke, A., 2002. Non-convex potentials and microstructures in finite strain plasticity. *Proc. R. Soc. Lond. A.* 458, 299–317.
- Cermelli, P., Gurtin, M. E., 2001. On the characterization of geometrically necessary dislocations in finite plasticity. *J. Mech. Physics Solids* 49 (7), 1539–1568.
- Chin, G. Y., Wonsiewicz, B. C., 1969. Deformation banding and the stability $\langle 100 \rangle$ – $\langle 111 \rangle$ fiber textures in FCC materials. *Trans. AIME* 245, 871–872.
- Christoffersen, H., Leffers, T., 1998. The orientation of dislocation walls in rolled copper relative to the sample coordinate system. *Acta mater.* 46 (12),

- 4093–4102.
- Conti, S., Ortiz, M., 2005. Dislocation microstructures and the effective behavior of single crystals. *Arch. Rational Mech. Anal.* 176 (1), 103–147.
- Evers, L. P., Parks, D., Brekelmans, W., Geers, M., 2002. Crystal plasticity model with enhanced hardening by geometrically necessary dislocation accumulation. *J. Mechanics Phys. Solids* 50 (11), 2403 – 2424.
- Godfrey, A., Hughes, D. A., 2000. Scaling of the spacing of deformation induced dislocation boundaries. *Acta metall. mater.* 48 (8), 1897–1905.
- Godfrey, A., Jensen, D. J., Hansen, N., 1998. Slip pattern, microstructure and local crystallography in an aluminum single crystal of copper orientation $\{112\}\langle 111 \rangle$. *Acta mater.* 46 (3), 835–848.
- Gurtin, M. E., 1981. *An introduction to continuum mechanics*. Academic Press, New York.
- Gurtin, M. E., 2002. A gradient theory of single-crystal viscoplasticity that accounts for geometrically necessary dislocations. *J. Mech. Phys. Solids* 50 (1), 5–32.
- Hirth, J. P., Lothe, J., 1992. *Theory of Dislocations*. Krieger.
- Huang, X., 1998. Grain orientation effect on microstructure in tensile strained copper. *Scripta mater.* 38 (11), 1697–1703.
- Huang, X., 2005. Extended dislocation boundaries in metals subjected to plane strain deformation. *Mater. Sci. Eng. A* 409, 52–58.
- Huang, X., Hansen, N., 1997. Grain orientation dependence of microstructure in aluminum deformed in tension. *Scripta mater.* 37 (1).
- Huang, X., Winther, G., 2007. Dislocation structures I: Grain orientation dependence. *Phil. mag.* 87 (33), 5189–5214.
- Hughes, D. A., Chrzan, D. C., Liu, Q., Hansen, N., 1998. Scaling of misorientation angle distributions. *Phy. rev. lett.* 81 (21), 4664–4667.

- Hughes, D. A., Hansen, N., 1993. Microstructural evolution in nickel during rolling from intermediate to large strains. *Met. Trans.* 24A (9), 2021–2037.
- Hughes, D. A., Liu, Q., Chrzan, D. C., Hansen, N., 1997. Scaling of microstructural parameters: Misorientations of deformation induced boundaries. *Acta mater.* 45 (1), 105–112.
- Humphreys, F. J., Bate, P. S., 2006. Measuring the alignment of low-angle boundaries formed during deformation. *Acta mater.* 54, 817–829.
- Hurley, P. J., Bate, P. S., Humphreys, F. J., 2003. An objective study of substructural boundary alignment in aluminium. *Acta mater.* 51 (16), 4737–4750.
- Hurley, P. J., Humphreys, F. J., 2003. The application of EBSD to the study of substructural development in a cold rolled single-phase aluminium alloy. *Acta mater.* 51 (4), 1087–1102.
- Hurtado, D. E., Ortiz, M., 2012. Surface effects and the size-dependent hardening and strengthening of nickel micropillars. *J. Mech. Phys. Solids* 60, 1432–1446.
- Kocks, U. F., Tomé, C. N., Wenk, H. R., 1998. *Texture and Anisotropy*. Cambridge University Press, Cambridge, U.K.
- Kuhlmann-Wilsdorf, D., Hansen, N., 1991. Geometrically necessary, incidental and subgrain boundaries. *Scripta Metallurgica et materialia* 25, 1557–1562.
- Kuroda, M., Tvergaard, V., 2007. Effects of texture on shear band formation in plane strain tension/compression and bending. *International journal of plasticity* 23 (2), 244–272.
- Lebensohn, R. E., Tomé, C. N., 1993. A self-consistent anisotropic approach for the simulation of plastic deformation and texture development of polycrystals: application to zirconium alloys. *Acta metall. mater.* 41 (9), 2611–2624.
- Leibfried, G., Breuer, N., Dederichs, P. H., 1978. *Point defects in metals*.

- Springer-Verlag (Berlin and New York).
- Lin, F. X., Godfrey, A., Winther, G., 2009. Grain orientation dependence of extended planar dislocation boundaries in rolled aluminium. *Scripta mater.* 61, 237–240.
- Liu, Q., Hansen, N., 1998. Macroscopic and microscopic subdivision of a cold-rolled aluminium single crystal of cubic orientation. *Proc. R. Soc. Lond. A* 454, 2555–2592.
- Liu, Q., Wert, J., Hansen, N., 2000. Location dependent lattice rotation and shear strain in rolled aluminum single crystals of cube and Goss orientations. *Acta mater.* 48, 4267–4279.
- Madec, R., Devincere, B., Kubin, L., Hoc, T., Rodney, D., 2003. The role of collinear interaction in dislocation-induced hardening. *Science* 301 (5641), 1879–1882.
- Mahesh, S., 2006. Deformation banding and shear banding in single crystals. *Acta mater.* 54 (17), 4565–4574.
- Mahesh, S., 2009. A hierarchical model for rate-dependent polycrystals. *Int. J. Plast.* 25 (5), 752–767.
- Mahesh, S., 2012. Orientation preferences of extended sub-granular dislocation boundaries. *Phil. Mag.* 92, 2286–2312.
- McCabe, R. J., Misra, A., Mitchell, T. E., 2004. Experimentally determined content of a geometrically necessary dislocation boundary in copper. *Acta mater.* 52, 705–714.
- Miehe, C., 2011. A multi-field incremental variational framework for gradient-extended standard dissipative solids. *J. Mech. Phys. Solids* 59 (4), 898–923.
- Miehe, C., Rosato, D., 2007. Fast texture updates in fcc polycrystal plasticity based on a linear active-set-estimate of the lattice spin. *J. Mech. Phys. Solids* 55 (12), 2687–2716.

- Morii, K., Mecking, H., Nakayama, Y., 1985. Development of shear bands in FCC single crystals. *Acta metall.* 33 (3), 379–386.
- Nicola, L., Van der Giessen, E., Gurtin, M. E., 2005. Effect of defect energy on strain-gradient predictions of confined single-crystal plasticity. *J. Mech. Phys. Solids* 53 (6), 1280–1294.
- Nye, J. F., March 1953. Some geometrical relations in dislocated crystals. *Acta metall.* 1, 153.
- Ortiz, M., Repetto, E. A., 1999. Nonconvex energy minimization and dislocation structures in ductile single crystals. *J. Mech. Phys. Solids* 47, 397–462.
- Ortiz, M., Repetto, E. A., Stainier, L., 2000. A theory of subgrain dislocation structures. *J. Mech. Phys. Solids* 48, 2077–2114.
- Pan, J., Rice, J. R., 1983. Rate-sensitivity of plastic flow and implications for yield-surface vertices. *Int. J. Solids Struct.* 19 (11), 973–987.
- Peeters, B., Kalidindi, S. R., Teodosiu, C., Houtte, P. V., Aernoudt, E., 2002. A theoretical investigation of the influence of dislocation sheets on evolution of yield surfaces in single-phase b.c.c. polycrystals. *J. Mech. Phys. Solids* 50 (4), 783 – 807.
- Sivakumar, S. M., Ortiz, M., 2004. Microstructure evolution in the equal channel angular extrusion process. *Comput. Methods Appl. Mech. Engrg.* 193 (48-51), 5177–5194.
- Steeds, J. W., 1966. Dislocation arrangement in copper single crystals as a function of strain. *Proc. R. Soc. Lond A.* 292, 343–373.
- Svendsen, B., 2002. Continuum thermodynamic models for crystal plasticity including the effects of geometrically-necessary dislocations. *J. Mech. Phys. Solids* 50 (6), 1297–1329.
- Taylor, G. I., 1938. Plastic strain in metals. *J. Inst. Met.* 62, 307.
- Van Houtte, P., Aernoudt, E., 1975. Solution of the generalized Taylor theory

- of plastic flow. I and II. *Z. Metallkde.* 66, 202–209.
- Wagner, P., Engler, O., Lücke, K., 1995. Formation of cu-type shear bands and their influence on deformation and texture of rolled FCC $\{112\}\langle 111\rangle$ single crystals. *Acta metall. mater.* 43 (10), 3799–3812.
- Wert, J. A., Huang, X., 2003. Extended planar boundary inclinations in FCC single crystals and polycrystals subjected to plane strain deformation. *Phil. Mag.* 83 (8), 969–983.
- Winther, G., 2003. Slip patterns and preferred dislocation boundary planes. *Acta mater.* 51, 417–429.
- Winther, G., 2008. Slip systems extracted from lattice rotations and dislocation structures. *Acta mater* 56 (9), 1919–1932.
- Winther, G., Huang, X., 2007. Dislocation structures II slip system dependence. *Phil. mag.* 87 (33), 5215–5235.
- Winther, G., Huang, X., Godfrey, A., Hansen, N., 2004. Critical comparison of dislocation boundary alignment studied by TEM and EBSD: technical issues and theoretical consequences. *Acta mater.* 52, 4437–4446.
- Winther, G., Huang, X., Hansen, N., 2000. Crystallographic and macroscopic orientation of planar dislocation boundaries – correlation with grain orientation. *Acta mater.* 48, 2187–2198.
- Winther, G., Jensen, D. J., Hansen, N., 1997. Dense dislocation walls and microbands aligned with slip planes – Theoretical considerations. *Acta mater.* 45 (12), 5059–5068.
- Wróbel, M., Dymek, S., Blicharski, M., Gorczyca, S., 1994. Dislocation microstructure and texture development in rolled copper single crystals. *Z. Metallkunde* 85 (6), 415–425.
- Yalcinkaya, T., Brekelmans, W., Geers, M., 2011. Deformation patterning driven by rate dependent non-convex strain gradient plasticity. *J. Mech.*

A Minimization of plastic power

A.1 Homogeneous grains

It is shown that subject to the constraint of Eq. (2), the plastic power $P(\dot{\gamma}_1, \dot{\gamma}_2, \dots, \dot{\gamma}_S)$, Eq. (7), of a homogeneous grain described in Sec. 2 achieves its minimum value when the slip-rates $\dot{\gamma}_s$ follow Eq. (3). To this end, consider the Lagrangian

$$L(\dot{\gamma}_1, \dot{\gamma}_2, \dots, \dot{\gamma}_S, \boldsymbol{\lambda}) = \sum_{s=1}^S \tau_s |\dot{\gamma}_s|^{1+1/n} + \boldsymbol{\lambda} : (\mathbf{D} - \sum_{s=1}^S \dot{\gamma}_s \mathbf{m}_s), \quad (\text{A.1})$$

where the first term on the right side is P and $\boldsymbol{\lambda}$ is the Lagrange multiplier for the constraint. Extrema of $L(\dot{\gamma}_1, \dot{\gamma}_2, \dots, \dot{\gamma}_S, \boldsymbol{\lambda})$ are characterized by

$$\frac{\partial L}{\partial \dot{\gamma}_t} = \tau_t (1 + 1/n) |\dot{\gamma}_t|^{1/n} \text{sign}(\dot{\gamma}_t) - \boldsymbol{\lambda} : \mathbf{m}_t = 0, \quad \forall t \in \{1, 2, \dots, S\}. \quad (\text{A.2})$$

Eq. (A.2) is satisfied for all t provided $\dot{\gamma}_t$ is given by Eq. (3) and $\boldsymbol{\lambda}$ is identified as

$$\boldsymbol{\lambda} = \boldsymbol{\sigma} (1 + 1/n). \quad (\text{A.3})$$

Further differentiating Eq. (A.2),

$$\frac{\partial^2 L}{\partial \dot{\gamma}_t \partial \dot{\gamma}_u} = \tau_t (1 + 1/n) (1/n) |\dot{\gamma}_t|^{1/n-1} \delta_{tu} \geq 0 \quad (\text{A.4})$$

is obtained. The positive definiteness of the Hessian $[\partial^2 L / \partial \dot{\gamma}_t \partial \dot{\gamma}_u]$ proves that the extremum obtained above is a minimum.

A.2 Banded grains

Subject to the constraint given by Eq. (17), $P(\dot{\gamma}_1^{(1)}, \dot{\gamma}_2^{(1)}, \dots, \dot{\gamma}_S^{(1)}, \dot{\gamma}_1^{(2)}, \dot{\gamma}_2^{(2)}, \dots, \dot{\gamma}_S^{(2)})$ will be minimized only when

$$\boldsymbol{\sigma}^{(1)} = \boldsymbol{\sigma}^{(2)}. \quad (\text{A.5})$$

The proof of this statement parallels that given in Appendix A.1 for the homogeneous grain. Consider the Lagrangian

$$L(\dot{\gamma}_1^{(1)}, \dot{\gamma}_2^{(1)}, \dots, \dot{\gamma}_S^{(1)}, \dot{\gamma}_1^{(2)}, \dot{\gamma}_2^{(2)}, \dots, \dot{\gamma}_S^{(2)}, \boldsymbol{\lambda}) = \frac{1}{2} \sum_{s=1}^S \tau_s |\dot{\gamma}_s^{(1)}|^{1+1/n} + \frac{1}{2} \sum_{s=1}^S \tau_s |\dot{\gamma}_s^{(2)}|^{1+1/n} + \boldsymbol{\lambda} : \left(\mathbf{D} - \frac{1}{2} \sum_{s=1}^S \dot{\gamma}_s^{(1)} \mathbf{m}_s^{(1)} - \frac{1}{2} \sum_{s=1}^S \dot{\gamma}_s^{(2)} \mathbf{m}_s^{(2)} \right).$$

The extrema of L are characterized by

$$\frac{\partial L}{\partial \dot{\gamma}_t^{(i)}} = (1/2)\tau_t(1 + 1/n)|\dot{\gamma}_t^{(i)}|^{1/n}\text{sign}(\dot{\gamma}_t^{(i)}) - (1/2)\boldsymbol{\lambda} : \mathbf{m}_t^{(i)} = 0, \quad (\text{A.6})$$

for all $t \in \{1, 2, \dots, S\}$ and for all $i \in \{1, 2\}$. Eq. (A.6) can be satisfied for all t and for both values of i by taking

$$\dot{\gamma}_t^{(i)} = \left| \frac{\boldsymbol{\sigma}^{(i)} : \mathbf{m}_t^{(i)}}{\tau_t} \right|^n \text{sign}(\boldsymbol{\sigma}^{(i)} : \mathbf{m}_t^{(i)}), \quad (\text{A.7})$$

and

$$\boldsymbol{\lambda} = \boldsymbol{\sigma}^{(1)}(1 + 1/n) = \boldsymbol{\sigma}^{(2)}(1 + 1/n). \quad (\text{A.8})$$

That the extremum obtained above is a minimum can be established by the positive definiteness of the Hessian $[\partial^2 L / \partial \dot{\gamma}_t \partial \dot{\gamma}_u]$ exactly as in Appendix. A.1. Eq. (A.8) immediately implies Eq. (A.5).